Physics – Uspekhi **62** (6) 568 – 595 (2019)

REVIEWS OF TOPICAL PROBLEMS PACS numbers: **12.39.–x**, 14.40.Lb, 14.40.Rt

X(3872) in the molecular model

Yu S Kalashnikova, A V Nefediev

DOI: https://doi.org/10.3367/UFNe.2018.08.038411

Contents

Abstract. We discuss methods and approaches for describing molecular states in the spectrum of heavy quarks and investigate various properties of the exotic charmonium-like state X(3872) in detail in the framework of the mesonic molecule model.

Keywords: phenomenology of strong interactions, exotic hadrons, threshold effect, charmonium, molecular model

1. Introduction

At the end of the 20th and early in this century, charmonium spectroscopy was considered a respectable but a somewhat dull subject. Indeed, since the charmonium revolution of 1974, all $\bar{c}c$ excitations below the open-charm threshold have been discovered, together with a fair amount of higher vector states directly accessible in the e^+e^- annihilation. With the advent of B-factories, everybody anticipated an observation of other higher $\bar{c}c$ charmonia; however, no surprises were expected from the theoretical standpoint: nonrelativistic Cornell-like quark models [1] seemed to be quite adequate for describing the spectra and radiative transitions of the observed charmonia. It appears, however, that it was premature to assume that we had fully understood the physics of the charmonium: experimental developments at B-factories revealed a bunch of states that, on the one hand, definitely contained a $\bar{c}c$ pair but, on the other hand, could not be described with a simple quark–antiquark assignment. In the literature, such states are conventionally referred to as exotic. To see the considerable progress achieved recently in studies of exotic charmonium-like states, it is sufficient to address review paper [2], which contains a brilliant description of the situation with exotic hadrons at the end of the first decade of the 21st century. In particular, the number of exotic states known at that time was fewer than ten, while now the total number of claimed exotic states in the spectrum of the charmonium exceeds 20, and approximately half of them are regarded as well established.

The first and best-studied representative of this family is the state X(3872), observed in 2003 by the Belle Collaboration in the reaction $B^+ \to K^+X \to K^+(\pi^+\pi^- J/\psi)$ [3]. We first note that this state lies fantastically close to the $D^0\bar{D}^{*0}$ threshold: for the average value of the mass, we have [4]

$$M_X = 3871.69 \pm 0.17 \text{ MeV}, \tag{1}$$

which is within just 1 MeV of the $D^0\bar{D}^{*0}$ threshold [4]:

$$E_b = M_{D^0} + M_{\bar{D}^{*0}} - M_X = -(1.1^{+0.6+0.1}_{-0.4-0.3}) \text{ MeV}. \tag{2}$$

Only an upper bound on the X(3872) total width exists [4]:

$$\Gamma_X < 1.2 \text{ MeV}. \tag{3}$$

Similarly, only an upper limit is imposed by the BABAR Collaboration on the total X(3872) production branching

Yu S Kalashnikova [(1,2,*)], **A V Nefediev** [(2,†)]
[(1)] National Research Center Kurchatov Institute, Alikhanov Institute of Theoretical and Experimental Physics, ul. B. Cheremushkinskaya 25, 117218 Moscow, Russian Federation
[(2)] Lebedev Physical Institute, Russian Academy of Sciences, Leninskii prosp. 53, 119991 Moscow, Russian Federation
E-mail: * yulia@itep.ru, † nefediev@itep.ru

Received 26 April 2018, revised 12 August 2018
Uspekhi Fizicheskikh Nauk **189** (6) 603 – 634 (2019)
DOI: https://doi.org/10.3367/UFNr.2018.08.038411
Translated by A V Nefediev; edited by A M Semikhatov

fraction in weak decays of the B-meson [5]:

$$\mathrm{Br}(\mathrm{B} \to \mathrm{KX}) < 2.6 \times 10^{-4}\,. \tag{4}$$

Later, this state was found in the $\pi^+\pi^-\pi^0\mathrm{J}/\psi$ mode [6], and it turned out that the two-pion and three-pion branchings were of the same order of magnitude:

$$\frac{\mathrm{Br}\,(\mathrm{X} \to \pi^+\pi^-\pi^0\mathrm{J}/\psi)}{\mathrm{Br}\,(\mathrm{X} \to \pi^+\pi^-\mathrm{J}/\psi)} = 1.0 \pm 0.4 \pm 0.3\,. \tag{5}$$

The latest results for the branching fractions are

$$\begin{aligned}\mathrm{Br}\big(\mathrm{B}^+ \to \mathrm{K}^+\mathrm{X}(3872)\big)\mathrm{Br}\big(\mathrm{X}(3872) \to \pi^+\pi^-\mathrm{J}/\psi\big) \\ = \big[8.63 \pm 0.82(\mathrm{stat.}) \pm 0.52(\mathrm{syst.})\big] \times 10^{-6}\,, \\ \mathrm{Br}\big(\mathrm{B}^0 \to \mathrm{K}^0\mathrm{X}(3872)\big)\mathrm{Br}\big(\mathrm{X}(3872) \to \pi^+\pi^-\mathrm{J}/\psi\big) \\ = \big[4.3 \pm 1.2(\mathrm{stat.}) \pm 0.4(\mathrm{syst.})\big] \times 10^{-6}\end{aligned} \tag{6}$$

for the dipion mode [7], and

$$\begin{aligned}\mathrm{Br}\big(\mathrm{B}^+ \to \mathrm{K}^+\mathrm{X}(3872)\big)\mathrm{Br}\big(\mathrm{X}(3872) \to \pi^+\pi^-\pi^0\mathrm{J}/\psi\big) \\ = \big[0.6 \pm 0.2(\mathrm{stat.}) \pm 0.1(\mathrm{syst.})\big] \times 10^{-5}\,, \\ \mathrm{Br}\big(\mathrm{B}^0 \to \mathrm{K}^0\mathrm{X}(3872)\big)\mathrm{Br}\big(\mathrm{X}(3872) \to \pi^+\pi^-\pi^0\mathrm{J}/\psi\big) \\ = \big[0.6 \pm 0.3(\mathrm{stat.}) \pm 0.1(\mathrm{syst.})\big] \times 10^{-5}\end{aligned} \tag{7}$$

for the tripion mode [8]. Studies of the pion spectra have shown that the dipion in the $\pi^+\pi^-\mathrm{J}/\psi$ mode originates from the ρ meson, while the tripion in the $\pi^+\pi^-\pi^0\mathrm{J}/\psi$ mode originates from the ω meson. For this reason, the two- and three-pion modes are respectively referred to as the $\rho\mathrm{J}/\psi$ and $\omega\mathrm{J}/\psi$ modes in what follows.

The threshold proximity of the X(3872) raises a burning question of the $\mathrm{D}^0\bar{\mathrm{D}}^{*0}$ mode. Indeed, such a mode was found in the B-meson decay $\mathrm{B}^+ \to \mathrm{K}^+\mathrm{D}^0\bar{\mathrm{D}}^0\pi^0$ [9] with a rather large branching fraction [1]

$$\mathrm{Br}\,(\mathrm{B}^+ \to \mathrm{K}^+\mathrm{D}^0\bar{\mathrm{D}}^0\pi^0) = (1.07 \pm 0.31^{+0.19}_{-0.33}) \times 10^{-4}\,. \tag{8}$$

The first measurements gave a somewhat higher mass than that found in the inelastic modes with hidden charm: the value

$$M_{\mathrm{X}} = 3875.2 \pm 0.7^{+0.3}_{-1.6} \pm 0.8\ \mathrm{MeV} \tag{9}$$

was presented in Ref. [9]. A more recent Belle result for the X(3872) mass in the $\mathrm{D}\bar{\mathrm{D}}^*$ mode is [10]

$$M_{\mathrm{X}} = 3872.9^{+0.6+0.4}_{-0.4-0.5}\ \mathrm{MeV}. \tag{10}$$

Although the BABAR Collaboration also gives a somewhat higher value for the mass in this mode than in the dipion mode [11], it is commonly accepted that this is the same state.

The value in (8) implies that X(3872) is produced in B-meson decays with branching fractions of the same order of magnitude as ordinary $\bar{\mathrm{c}}\mathrm{c}$ charmonia are [4]:

$$\mathrm{Br}(\mathrm{B} \to \mathrm{KJ}/\psi, \mathrm{K}\psi', \mathrm{K}\chi_{\mathrm{c1}}) \sim 10^{-4}\,. \tag{11}$$

[1] Data on the open-charm modes are presented in different ways by different collaborations. Belle presents the data on the $\mathrm{D}\bar{\mathrm{D}}\pi$ channel, while BABAR sums the data obtained for the $\mathrm{D}\bar{\mathrm{D}}\pi$ and $\mathrm{D}\bar{\mathrm{D}}\gamma$ final states and refers to the corresponding mode as $\mathrm{D}\bar{\mathrm{D}}^*$. To simplify the notation, the open-charm channel is labeled as $\mathrm{D}\bar{\mathrm{D}}^*$ in what follows, irrespective of the particular collaboration.

This state is also observed in the radiative modes. The BABAR Collaboration gives the $\gamma\mathrm{J}/\psi$ and $\gamma\psi'$ modes [12]

$$\begin{aligned}\mathrm{Br}(\mathrm{B}^\pm \to \mathrm{K}^\pm\mathrm{X})\mathrm{Br}(\mathrm{X} \to \gamma\mathrm{J}/\psi) = (2.8 \pm 0.8 \pm 0.2) \times 10^{-6}\,, \\ \mathrm{Br}(\mathrm{B}^\pm \to \mathrm{K}^\pm\mathrm{X})\mathrm{Br}(\mathrm{X} \to \gamma\psi') = (9.5 \pm 2.9 \pm 0.6) \times 10^{-6}\,,\end{aligned} \tag{12}$$

and the ratios

$$\frac{\mathrm{Br}(\mathrm{X} \to \gamma\mathrm{J}/\psi)}{\mathrm{Br}(\mathrm{X} \to \pi^+\pi^-\mathrm{J}/\psi)} = 0.33 \pm 0.12\,, \tag{13}$$

$$\frac{\mathrm{Br}(\mathrm{X} \to \gamma\psi')}{\mathrm{Br}(\mathrm{X} \to \pi^+\pi^-\mathrm{J}/\psi)} = 1.1 \pm 0.4\,. \tag{14}$$

The data from the Belle Collaboration are [13]

$$\begin{aligned}\mathrm{Br}(\mathrm{B}^\pm \to \mathrm{K}^\pm\mathrm{X})\mathrm{Br}(\mathrm{X} \to \gamma\mathrm{J}/\psi) = (1.78^{+0.48}_{-0.44} \pm 0.12) \times 10^{-6}, \\ \mathrm{Br}(\mathrm{B}^\pm \to \mathrm{K}^\pm\mathrm{X})\mathrm{Br}(\mathrm{X} \to \gamma\psi') < 3.45 \times 10^{-6}\,,\end{aligned} \tag{15}$$

and hence there is a discrepancy between the two collaborations on the $\gamma\psi'$ mode. There is also a recent measurement of the ratio of the branching fractions for the given modes, performed by the LHCb Collaboration [14]:

$$R \equiv \frac{\mathrm{Br}(\mathrm{X} \to \gamma\psi')}{\mathrm{Br}(\mathrm{X} \to \gamma\mathrm{J}/\psi)} = 2.46 \pm 0.64 \pm 0.29\,. \tag{16}$$

The story of the X(3872) quantum numbers is rather dramatic. Studies of the dipion mode performed by the CDF at the Tevatron [15] allowed restricting the quantum numbers of X(3872) to only two options: 1^{++} or 2^{-+}. There are good phenomenological reasons to assign the X(3872) 1^{++} quantum numbers, and hence the 1^{++} option became more popular. However, the BABAR analysis [8] resulted in the conclusion that the $\pi^+\pi^-\pi^0$ mass distribution was described better with the angular momentum $L = 1$ in the $\omega\mathrm{J}/\psi$ system than with the angular momentum $L = 0$. The former implies a negative P-parity for X(3872) and therefore entails the 2^{-+} assignment. Meanwhile, it is shown in Ref. [16] that if a combined analysis of the data obtained at B-factories for both two-pion and three-pion modes is performed, then the 1^{++} option is preferable. It was only in 2013 that it became possible to reject (at the 8σ level) the 2^{-+} hypothesis, due to high-statistics measurements of the two-pion mode performed in the LHCb experiment at CERN [17, 18].

With the 1^{++} quantum numbers, the most natural possibility for X(3872) is the genuine $2^3\mathrm{P}_1$ $\bar{\mathrm{c}}\mathrm{c}$ charmonium; however, this possibility seems to be ruled out by the mass argument: the quark model calculations give a higher value for the mass of the $2^3\mathrm{P}_1$ state (see, e.g., Refs [19–21]). Moreover, ratio (5) of the branchings for the $\rho\mathrm{J}/\psi$ and $\omega\mathrm{J}/\psi$ modes indicates a strong isospin symmetry violation, which is difficult to explain in the framework of a simple $\bar{\mathrm{c}}\mathrm{c}$ model.

There is no deficit of models for X(3872), as we show in Fig. 1, where models discussed in the literature are depicted

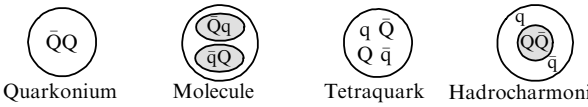

Figure 1. Models of X(3872) compatible with the 1^{++} quantum numbers.

schematically. One of them, the hadronic molecule model, has a quite long history (see, e.g., [22, 23]), and the discovery of the X(3872) state at the $D\bar{D}^*$ threshold made this model quite popular again [24–29]. We note that in the molecular model, the aforementioned isospin symmetry violation in X(3872) decays appears in a natural way [30, 31]. Another popular model for X(3872) is the tetraquark model (see [32–35]). Finally, a recent arrival is the hadrocharmonium model [36, 37], which offers a natural explanation of the high probability of the exotic state decaying into a lower charmonium plus light hadrons.

Generally speaking, the wave function of X(3872) must contain, in addition to the genuine $\bar{c}c$ component, extra components like $D\bar{D}^*$ molecular ones, a tetraquark, a $\bar{c}cg$ hybrid, and others, whose nature is unclear. The relative weights of all these components are to be determined dynamically and, in the absence of an analytic solution of QCD, are very model-dependent. However, for a near-threshold resonance, it is possible to define the admixture of a hadronic molecule in the wave function of the resonance in a model-independent way [38–40]. In this review, we argue that in the case of the X(3872) state, we can indeed estimate this admixture using the aforementioned approach and demonstrate that the molecular $D\bar{D}^*$ component dominates the X(3872) wave function. We also discuss various scenarios of the formation of such a mesonic molecule and the role of the molecular component played in the pionic and radiative decays the X(3872).

It is worth noting that papers on X(3872) are still the most cited publications of the Belle Collaboration since it was established. This is not only because the X(3872) state is interesting in and of itself. We have already mentioned that the spectroscopy of heavy-quark flavors is experiencing a renaissance because the experiment constantly brings information on new states that do not fit into the quark model scheme. At the same time, the molecular model is one of the most successful approaches that allows qualitatively (and in some cases quantitatively) explaining the properties of such exotic states in the spectrum of heavy quarks and predicting new resonances. The interested reader can find a detailed discussion of this model applied to hadronic spectroscopy in a recent review [41]. We mention only two such applications closely related to X(3872).

The first deals with so-called Z resonances, which are charged and do not therefore allow a simple quark–antiquark interpretation; obviously, their minimal quark content is four-quark. The Z states in the spectrum of charmonium, conventionally denoted as Z_c, lie near strong thresholds and therefore give good reason to be interpreted as hadronic molecules. In particular, the state $Z_c(3900)$ observed by BES III [42] and Belle [43] is often discussed in the literature as an isovector $D\bar{D}^*$ molecule with the quantum numbers $J^{PC} = 1^{+-}$, i.e., as a spin partner of X(3872). Remarkably, analogous charged Z states were recently found in the spectrum of bottomonium: these are the so-called $Z_b(10610)$ and $Z_b(10650)$, lying near the respective $B\bar{B}^*$ and $B^*\bar{B}^*$ thresholds [44, 45]. A molecular interpretation of these states is suggested in [46] and further developed in a series of later studies.

The other application to be mentioned is related to transitions between molecular states, in particular, involving exotic vector charmonia, traditionally denoted as Y's. One of the best-studied Y resonances is the Y(4260) observed by BABAR in the channel $J/\psi\pi^+\pi^-$ [47]. This state is not seen in the inclusive cross section of $e^+e^- \to$ hadrons, which has no satisfactory explanation for a genuine $\bar{c}c$ charmonium, and the proximity of its mass to the $D_1\bar{D}$ threshold hints at a large admixture of the hadronic component in its wave function, i.e., its possible molecular nature [48–51]. The assumption that Y(4260) is a $D_1\bar{D}$ molecule while $Z_c(3900)$ is a $D\bar{D}^*$ one allows a nice model to be developed for the decay $Y(4260) \to \pi Z_c(3900)$ (see paper [48]). The radiative transition $Y(4260) \to \gamma X(3872)$ can be described similarly [52].

We might be witnessing the beginning of a new molecular spectroscopy. The X(3872) state is an ideal (at least, the best possible so far) laboratory to study exotic molecules. On the one hand, vast experimental materials on it exist. On the other hand, this is a typical near-threshold resonance containing heavy quarks. As a result, X(3872) allows using the full power of theoretical and phenomenological approaches developed so far to extract all possible information on the nature and properties of this state from the experimental data and to identify the interactions responsible for its formation. This paper is therefore devoted to a review of various methods and approaches used in the molecular model and an illustration of their practical application using the example of the best-studied state X(3872). Systematization of our knowledge on exotic near-threshold states is particularly relevant and timely now in view of the launch of the upgraded B-factory Belle-II, as well as plans for the super-c-τ factory construction in Novosibirsk. The physical programs of both experiments contain investigations in hadronic spectroscopy.

To make reading this review easier, we collect all the definitions and conventions used in it in Section 2, which also contains a justification of a dedicated study of near-threshold states. Wherever appropriate, each section containing a large amount of technical details and formulas begins with a short introduction to the physical results discussed in that section. The reader whose aim is to become generally acquainted with the subject of the review, with technical details being unimportant, can skip most of the formulas in Section 2; for this, we provide brief instructions on what can and what cannot be skipped on the first reading. We also spotlight important conclusions that cannot be skipped.

2. Definitions and conventions

We start by explaining some notions used in this review. The word 'resonance' is used as a synonym for 'state'. Such an identification is motivated by the fact that each state has decay channels and therefore the corresponding pole always resides on an unphysical sheet of the Riemann surface, away from the real axis (the Schwarz reflection principle requires that a symmetric 'mirror' pole also exist, whose imaginary part has the opposite sign). In other words, such a state cannot be regarded as bound or virtual in the proper sense of the word. Nevertheless, it is convenient to use the terminology of bound and virtual states from the standpoint of the pole location near a given threshold and on the corresponding Riemann surface sheet with respect to this threshold. We consider a simple example. For n decay channels, the Riemann surface for the state under study is multi-sheeted, with the number of sheets equal to 2^n. However, if only a limited region near a given threshold is considered while all other thresholds can be viewed as remote, it is sufficient to confine oneself to a double-sheeted Riemann surface for the nearest threshold and regard one of the sheets as physical (it turns into a genuine physical sheet as the coupling to all other

channels is switched off) and the other as unphysical. With such a definition, a below-threshold pole lying on the physical sheet of such a double-sheeted Riemann surface is conventionally called a bound state, while a similar pole on the unphysical sheet is called a virtual state, although in either case the pole is somewhat shifted away from the real axis. It is important to note that from the standpoint of the full multi-sheeted Riemann surface, both aforementioned sheets are unphysical, and therefore shifting poles to the complex plane does not result in a contradiction with the probability conservation or other basic principles of quantum mechanics.

All decay channels of the studied resonance can be divided into 'elastic' or 'inelastic', which are strong decays into a respective open-flavor or hidden-flavor final state; the corresponding thresholds are also called elastic and inelastic. All elastic channels considered in this review are assumed to be S-wave, while there is no constraint on the relative momentum in the inelastic channels. A state residing at a strong threshold is referred to as a near-threshold state, and the energy region around this threshold is called a near-threshold region. The size of such a region can be defined for each particular problem under study; however, in any case, it is bounded by the nearest elastic and inelastic thresholds.

We say that a state whose structure exerts no influence on the effect under study, for example, the line shape of a near-threshold resonance, is 'elementary' or 'bare'. In many cases, the elementary state can be understood as a compact quark compound, for example, a genuine quarkonium, tetraquark, hybrid, and so on. Then the hard scale that governs the behavior of the transition form factors between different channels of the reaction and which is defined by the binding forces of the corresponding state is called the (inverse) range of force. For example, the inverse range β of the force for the coupling of an elementary state to a hadronic channel is defined by the interquark interaction responsible for the formation of this elementary state. Unless stated otherwise, it is assumed that $\beta \simeq 1$ GeV and that it exceeds all typical momenta in the problem. The corresponding effective field theory is built in the leading order in the expansion in the inverse range of force. Finally, a near-threshold state whose wave function is dominated by the hadronic component is said to be a 'molecular' state. The nature of such a molecule is not specified: a full variety of options is allowed for it, from a bound or virtual state to an above-threshold resonance. In a similar way, possible binding forces in the molecule are not limited to the t-channel exchanges and can have different origins; establishing the nature of such forces is one of the most important problems in the phenomenology of near-threshold states.

Finally, we comment on the applicability of the terms 'mass' and 'width' for near-threshold states. A fundamental characteristic of a resonance is the location of its pole in the complex plane. In practice, the location of this pole may not be possible to determine in the case of a multi-sheeted Riemann surface and in the presence of strongly coupled channels. On the other hand, the mass and the width are standard parameters of the Breit–Wigner distribution, which is quite successful in describing isolated resonances, i.e., the states in the spectrum lying sufficiently far from other states and from thresholds of the channels with the given quantum numbers.

As an example, we consider the S-matrix element describing the scattering of heavy–light mesons on each other, $(\bar{\mathrm{Q}}\mathrm{q}) + (\bar{\mathrm{q}}\mathrm{Q}) \to (\bar{\mathrm{Q}}\mathrm{q}) + (\bar{\mathrm{q}}\mathrm{Q})$ (here, Q and q are the respective heavy and light quark), and express it through the amplitude A as

$$S = 1 + 2\mathrm{i}A\,. \tag{17}$$

Then the unitarity requires the condition

$$AA^\dagger = \frac{1}{2\mathrm{i}}\,(A - A^\dagger) \tag{18}$$

to hold, which is satisfied automatically if a real quantity K (in a multichannel case, K is a Hermitian matrix) is introduced as

$$A = K(1 - \mathrm{i}K)^{-1}. \tag{19}$$

If scattering proceeds through the formation of a resonance, the function K can be written in the form

$$K = G(s)\,\frac{1}{M^2 - s}\,G(s) = \frac{\Gamma(s)\sqrt{s}}{M^2 - s}, \quad \Gamma(s) = \frac{G^2(s)}{\sqrt{s}}\,, \tag{20}$$

where s is the invariant energy and we introduce the vertex function $G(s)$ and the parameter M that respectively define the coupling of the resonance to the hadronic channel and its propagation function. Then, with the help of Eqn (19) we can obtain

$$A = \frac{\Gamma(s)\sqrt{s}}{M^2 - s - \mathrm{i}\Gamma(s)\sqrt{s}}\,. \tag{21}$$

We consider a region in the vicinity of the resonance $s \sim M^2$. If the vertex function is nearly a constant in this region, i.e., we can set $\Gamma(s) \approx \Gamma(M^2) \equiv \Gamma$, and $\Gamma \ll M$, then amplitude (21) can be expanded with only the leading term retained,

$$A \approx \frac{\Gamma/2}{M - \sqrt{s} - \mathrm{i}\Gamma/2}\,. \tag{22}$$

The distribution thus obtained is the celebrated Breit–Wigner distribution, and the quantities M and Γ are known as the mass and the width of the resonance.

If the resonance resides near a threshold, i.e., $M \simeq 2M_{\bar{\mathrm{Q}}\mathrm{q}} \equiv M_{\mathrm{th}}$, then the dependence of the vertex function on the energy is important and cannot be ignored. As a result, the line shape of a near-threshold resonance is not described by the Breit–Wigner distribution. Furthermore, the notions of the mass and width cannot be defined for it. Indeed, near the threshold, the width of a two-body S-wave decay behaves as $\Gamma \propto \sqrt{E}$, where the energy E is measured relative to the threshold M_{th}, i.e., $\sqrt{s} = M_{\mathrm{th}} + E$. Then amplitude (22) takes the form

$$A \propto \frac{1}{E - E_0 + \mathrm{i} \times \mathrm{const} \times \sqrt{E}}\,, \tag{23}$$

where we set $E_0 = M - M_{\mathrm{th}}$ for convenience. It is easy to see that distribution (23) has few features not inherent in Breit–Wigner distribution (22), namely

- the line shape is asymmetric with respect to $E = E_0$;
- the maximum of the curve does not necessarily lie at E_0, because the function $\sqrt{E}$ must be analytically continued below the threshold, i.e., to $E < 0$, where it contributes to the real part of the denominator and shifts the pole;

• for a particular relation between the parameters, the peak resides strictly at the threshold, i.e., at $E = 0$, irrespective of the value taken by the parameter E_0;

• the visible width of the peak is not given by a single parameter, like the width Γ in formula (22), which would define the imaginary part of the pole position in the complex energy plane;

• the derivative of the amplitude with respect to energy is infinite at the threshold.

These properties of distribution (23) are threshold phenomena, which constitute the subject of this review. In particular, in Section 3.3 we consider the form of the distributions for near-threshold states resulting from the interplay of different dynamics, including the multichannel case.

As was mentioned above, it is not possible as a matter of principle to introduce the notions of mass and width for a near-threshold state. We note that the X(3872) mass quoted in Eqn (1) should not be taken literally, because it was obtained from a Breit–Wigner fit for the line shape. The most important information encoded in Eqn (2) is that X(3872) resides very close to the neutral two-body threshold $D\bar{D}^*$, and therefore taking it into account is critically important for understanding the nature of this state.

Also, it proves convenient to deal with the notion of the binding energy, which should therefore be properly defined. It follows from the foregoing that the simple method used in formula (2) is inapplicable in view of the uncertainty in the definition of the mass M_X. In what follows, by the energy of a near-threshold state, we understand the difference between the zero of the real part of the denominator of the distribution and the threshold position (in other words, this is the real part of the pole of the amplitude relative to the threshold). At the same time, convenient and universal parameters describing the imaginary part of the denominator are the coupling constants of the resonance to its various decay channels.

We also note that Breit–Wigner amplitude (22) has only one pole in the complex energy plane, which lies at $E = E_0 - i\Gamma/2$. Formally, this contradicts the Schwarz reflection principle and thus violates the analyticity of the amplitude. However, this violation is not large if we consider the energy region near the resonance, because the path of the mirror pole, located at $E_0 + i\Gamma/2$, to this region is much longer than that of the pole at $E_0 - i\Gamma/2$. At the same time, when working near the threshold, we have to retain both symmetric poles, because neither of them can be regarded as dominating in this region. Obviously, amplitude (22) does not satisfy this requirement and has to be generalized.

3. Elementary or compound state?

As mentioned in the Introduction, the wave function of a near-threshold resonance can contain both a compact, 'elementary', and a molecular component. Investigating the nature of such a resonance includes, inter alia, establishing the relative weights of these components in a model-independent way. The cornerstone of the method suggested by Weinberg in his studies [38–40] is the analysis of low-energy observables, which indeed allows making conclusions as to whether a given state is 'elementary' or compound.

Weinberg's method is based on the idea of extending the basis of the coupled channels to include the 'bare' resonance whose wave function is renormalized because of the interaction with the 'compound' channels. Ideologically, this method is reminiscent of the standard field theoretical approach, where the interaction of fields results in a decrease in the probability of observing the 'bare' field from unity to a smaller value $0 \leqslant Z \leqslant 1$. An important achievement gained in Weinberg's approach is establishing a one-to-one correspondence between such a Z factor and experimentally observable quantities, which eventually allows coming to a model-independent conclusion on the structure of the wave function of the resonance.

In [40], this approach was applied to the case of a below-threshold state, the deuteron. In [53], a natural generalization of this approach to the case of an arbitrary near-threshold resonance was suggested, equally applicable to both below- and above-threshold resonances; it also allowed incorporating inelasticity. It is important to note that the most relevant formalism to be used with the Weinberg approach is the t-matrix (or scattering operator) approach, brilliantly described in book [54], after it is extended to include the 'elementary' state. Details of this generalized formalism considered in this section can be found in Refs [55, 56]

In Section 3.1, the reader should pay attention to the formulation of the coupled-channel problem [Eqns (24)–(26)], to the different types of solutions of such a problem [Eqns (38) and (41)], and to the definition of the Z factor [Eqn (40)] and the spectral density as its convenient generalization [Eqn (42)], which are used in the analysis of the experimental data for X(3872) in what follows. In Section 3.2, important information is contained in Weinberg formulas (59) and (60), as well as in Eqn (66), which gives the most general form of the energy distribution for a single hadronic channel with direct interaction between mesons in it.

In Section 3.3, we describe a generalization of the results in Section 3.2 to the two-channel case. The main results in this subsection are illustrated in Figs 3–5, the most important conclusion being the observation that quite a nontrivial line shape of a near-threshold resonance can be provided by only two parameters defining the position of the zero of the scattering amplitude and the contribution of the nonlinear term $k_1 k_2$, where k_1 and k_2 are the momenta in the mesonic channels. Because the existing experimental data on X(3872) do not allow such irregularities of the line shape to be identified, Section 3.3 provides a surplus to be used in the future, when new experiments are able to provide us with accurate information on near-threshold states containing heavy quarks. This part can be skipped during cursory reading of this review or if the reader is only interested in the state-of-the-art of the experimental situation with X(3872).

3.1 Coupled-channel scheme

We consider a physical resonance that is a mixture of a bare elementary state $|\psi_0\rangle$ (for example, $\bar{c}c$ or a tetraquark) and multiple two-body components (labeled as $i = 1, 2, \ldots$), and represent its wave function as

$$|\Psi\rangle = \begin{pmatrix} c|\psi_0\rangle \\ \chi_1(\mathbf{p})|\, M_{11} M_{12}\rangle \\ \chi_2(\mathbf{p})|\, M_{21} M_{22}\rangle \\ \cdots \end{pmatrix}, \tag{24}$$

where c is the probability amplitude for the bare state, and $\chi_i(\mathbf{p})$ describes the relative motion in the system of two

mesons $\{M_{i1}M_{i2}\}$ with the relative momentum $\mathbf{p}$. The system is described by the Schrödinger equation

$$\mathcal{H}|\Psi\rangle = M|\Psi\rangle \tag{25}$$

with the Hamiltonian

$$\hat{\mathcal{H}} = \begin{pmatrix} H_0 & V_{01} & V_{02} & \cdots \\ V_{10} & H_{\rm h1} & V_{12} & \cdots \\ V_{20} & V_{21} & H_{\rm h2} & \cdots \\ \cdots & \cdots & \cdots & \cdots \end{pmatrix}. \tag{26}$$

We have $H_0|\psi_0\rangle = M_0|\psi_0\rangle$, where M_0 is the mass of the bare state. In what follows, it is convenient to work in terms of the energy measured from the lowest threshold with $i = 1$:

$$M = m_{11} + m_{12} + E\,, \qquad M_0 = m_{11} + m_{12} + E_0\,.$$

We assume direct interactions between mesonic channels i and j to exist and encode them in the potentials $V_{ij}(\mathbf{p},\mathbf{p}')$ (including the diagonal terms with $i = j$), such that

$$H_{{\rm h}i}(\mathbf{p},\mathbf{p}') = \left(m_{i1} + m_{i2} + \frac{p^2}{2\mu_i}\right)\delta^{(3)}(\mathbf{p}-\mathbf{p}') + V_{ii}(\mathbf{p},\mathbf{p}')\,,$$

where m_{i1} and m_{i2} are the meson masses in the ith channel, with the reduced mass

$$\mu_i = \frac{m_{i1}m_{i2}}{m_{i1}+m_{i2}}\,.$$

The ith mesonic channel and the bare state communicate via the off-diagonal quark–meson potential V_{0i}, which is given by the transition vertex $f_i(\mathbf{p})$.

The t-matrix for the coupled-channel problem satisfies the Lippmann–Schwinger equation (written schematically)

$$t = V - VSt\,, \tag{27}$$

where S is the diagonal matrix of free propagators,

$$S_0(E) = \frac{1}{E_0 - E - {\rm i}0}\,, \tag{28}$$

$$S_i(\mathbf{p}) = \frac{1}{p^2/(2\mu_i) - E + \Delta_i - {\rm i}0}\,, \tag{29}$$

$$\Delta_i = (m_{i1} + m_{i2}) - (m_{11} + m_{12})\,.$$

The formalism of the t-matrix is of course fully equivalent to a more 'standard' method based on the Schrödinger equation for the wave function of the system (see, e.g., textbook [57]). Nevertheless, the t-matrix (or the scattering matrix, as it is sometimes called in the literature; see, e.g., book [54]) grants some advantages. In particular, it allows one to consider the scattering problem for an off-shell particle, i.e., to formally 'disentangle' the momentum and the energy, which for on-shell particles are linked to each other via the dispersion relation.

As the first step, it is convenient to define the t-matrix for the potential problem (that is, the t-matrix of the direct interaction in the mesonic channel t^V) which satisfies the equation

$$t^V_{ij}(\mathbf{p},\mathbf{p}') = V_{ij}(\mathbf{p},\mathbf{p}') - \sum_k \int V_{ik}(\mathbf{p},\mathbf{q})S_k(\mathbf{q})t^V_{kj}(\mathbf{q},\mathbf{p}')\,{\rm d}^3q \tag{30}$$

and introduce the dressed vertex functions

$$\phi_i(\mathbf{p}) = f_i(\mathbf{p}) - \sum_k \int t^V_{ik}(\mathbf{p},\mathbf{q})S_k(\mathbf{q})f_k(\mathbf{q})\,{\rm d}^3q\,, \tag{31}$$

$$\bar{\phi}_i(\mathbf{p}') = f_i(\mathbf{p}) - \sum_k \int S_k(\mathbf{q})f_k(\mathbf{q})t^V_{ki}(\mathbf{q},\mathbf{p}')\,{\rm d}^3q\,. \tag{32}$$

In terms of these quantities, the full t-matrix can be expressed as [56]

$$t_{00}(E) = -\frac{(E-E_0)\mathcal{G}(E)}{E - E_0 + \mathcal{G}(E)}\,, \tag{33}$$

$$t_{0i}(\mathbf{p},E) = \frac{E-E_0}{E-E_0+\mathcal{G}(E)}\,\bar{\phi}_i(\mathbf{p})\,, \tag{34}$$

$$t_{i0}(\mathbf{p},E) = \frac{E-E_0}{E-E_0+\mathcal{G}(E)}\,\phi_i(\mathbf{p})\,, \tag{35}$$

$$t_{ij}(\mathbf{p},\mathbf{p}',E) = t^V_{ij}(\mathbf{p},\mathbf{p}') + \frac{\phi_i(\mathbf{p})\bar{\phi}_j(\mathbf{p}')}{E-E_0+\mathcal{G}(E)}\,, \tag{36}$$

where

$$\mathcal{G}(E) = \sum_i \int f_i^2(\mathbf{q})S_i(\mathbf{q})\,{\rm d}^3q - \sum_{i,j}\int f_i(\mathbf{k})S_i(\mathbf{k})t^V_{ij}(\mathbf{k},\mathbf{q})S_j(\mathbf{q})f_j(\mathbf{q})\,{\rm d}^3k\,{\rm d}^3q. \tag{37}$$

The system under consideration can have bound states (generally, more than one). For the αth bound state with the binding energy $E_{\rm b}^{(\alpha)}$, the solution of Eqn (35) can be written as

$$c_{\rm b}^{(\alpha)} = \cos\theta_\alpha\,, \quad \chi_{\rm b}^{(i\alpha)}(\mathbf{p}) = S_i(\mathbf{p})\phi_i(\mathbf{p})\sin\theta_\alpha\,. \tag{38}$$

The wave function of this bound state is normalized,

$${}^{(\alpha)}_{\rm b}\langle\Psi|\Psi\rangle^{(\alpha)}_{\rm b} = 1\,,$$

whence for the mixing angle θ_α we have the relation

$$\tan^2\theta_\alpha = \sum_i \int S_i^2(\mathbf{p})\phi_i^2(\mathbf{p})\,{\rm d}^3p\,. \tag{39}$$

The quantity

$$Z_\alpha = \left|\langle\psi_0|\Psi\rangle^{(\alpha)}_{\rm b}\right|^2 = \cos^2\theta_\alpha\,, \tag{40}$$

introduced in Ref. [40], gives the probability of finding a bare state in the wave function of the αth bound state.

The solution of Eqn (25) with the free asymptotic form in the hadronic channel i takes the form

$$\chi^{(i)}_{j;\mathbf{k}_i}(\mathbf{p}) = \delta_{ij}\delta^{(3)}(\mathbf{p}-\mathbf{k}_i) - S_j(\mathbf{p})t_{ji}(\mathbf{p},\mathbf{k}_i,E)\,, \qquad c^{(i)}_{\mathbf{k}_i}(E) = -\frac{t_{0i}(\mathbf{k}_i,E)}{E_0-E}\,, \tag{41}$$

where $k_i = \sqrt{2\mu_i(E-\Delta_i)}$. The solution for the coefficient c [see Eqn (41)] allows us to define a continuum counterpart of quantity (40) [the spectral density $w(E)$], which gives the probability of finding the bare state in the continuum wave

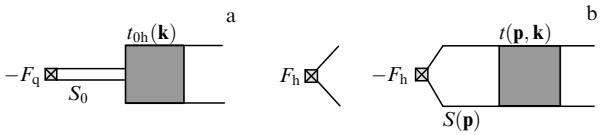

Figure 2. Diagrams of two-meson production (a) via the quark component and (b) via the hadronic component.

function [58]. It is given by

$$w(E) = \sum_i \mu_i k_i \Theta(E - \Delta_i) \int \left| c^{(i)}_{\mathbf{k}_i}(E) \right|^2 \mathrm{d}o_{\mathbf{k}_i}\,, \tag{42}$$

where Θ is the Heaviside function. As shown in Ref. [58], the normalization condition for the distribution $w(E)$ is

$$\int_0^\infty w(E)\,\mathrm{d}E = 1 - \sum_\alpha Z_\alpha\,, \tag{43}$$

where summation is over all bound states present in the system.

We conclude this subsection with the formulas for the production amplitude of the resonance under study. In fact, because the wave function of the system is multicomponent [see Eqn (24)], there are several production mechanisms possible: production of the resonance via its quark component or via its hadronic components, as depicted in Fig. 2. For our purposes, it is sufficient to consider a point-like production source. Then the production amplitude of the meson pair $(M_{i1}M_{i2})$ via the hadronic component j can be written as

$$\mathcal{M}^i_j(E) = \mathcal{F}_{\mathrm{h}j}\delta_{ij} - \mathcal{F}_{\mathrm{h}j} \int S_j(\mathbf{p}) t_{ji}(\mathbf{p}, \mathbf{k}_i, E)\,\mathrm{d}^3 p\,, \tag{44}$$

where $\mathcal{F}_{\mathrm{h}j}$ is the initial-state production amplitude from a point-like source, and $k_i = \sqrt{2\mu_i(E - \Delta_i)}$. The production amplitude from the quark component is given by

$$\mathcal{M}^i_{\mathrm{q}}(E) = -\mathcal{F}_{\mathrm{q}} S_0(E) t_{0i}(\mathbf{k}_i, E)\,, \tag{45}$$

where $\mathcal{F}_{\mathrm{q}}$ is the production amplitude for the bare quark state by a point-like source.

3.2 Weinberg formulas, singularity structure, and underlying dynamics

We consider a single mesonic channel (omitting the channel index) with the S wave in the mesonic subsystem, and take the low-energy limit defined by the inequality $k \ll \beta$, where k is the momentum in the mesonic subsystem and β is the inverse range of force.

For convenience, we define the loop functions

$$\begin{aligned} g(E) &= \int \mathrm{d}^3 q\, \frac{f^{\,2}(\mathbf{q})}{q^2/(2\mu) - E - \mathrm{i}0} = f_0^{\,2}(R + 4\pi^2\mu \mathrm{i}k)\,, \\ g'(E) &= \int \mathrm{d}^3 q\, \frac{f(\mathbf{q})}{q^2/(2\mu) - E - \mathrm{i}0} = f_0(R' + 4\pi^2\mu \mathrm{i}k)\,, \end{aligned} \tag{46}$$

where μ is the reduced mass. For the real parts of the loops, R and R', only the leading contributions of the order of $\mu\beta$ are retained, while the corrections $O(k^2/\beta^2)$ are disregarded; we also set $f_0 \equiv f(0)$. Using the scattering length approximation for the potential problem t-matrix,

$$t_V(\mathbf{q}, \mathbf{p}, E) = -\frac{1}{4\pi^2\mu(-a_V^{-1} - \mathrm{i}k)}\,, \tag{47}$$

where the scattering length a_V is treated as an input parameter, we arrive at the mesonic t-matrix element (36) in the form

$$\begin{aligned} t(E) &= \frac{E - E_{\mathrm{C}}}{[E - E_0]R_V + f_0^{\,2}[RR_V - R'^2] + 4\pi^2\mu \mathrm{i}k[E - E_{\mathrm{C}}]}\,, \\ E_{\mathrm{C}} &= E_0 - f_0^{\,2}(R + R_V - 2R')\,, \end{aligned} \tag{48}$$

where $R_V = (2\pi)^2\mu\gamma_V$, $\gamma_V = 1/a_V$. We note that expression (48) for the mesonic t-matrix has a zero at the energy $E = E_{\mathrm{C}}$, which is discussed in detail in Section 3.3.

Expression (48) allows performing a renormalization procedure, i.e., redefining the 'bare' parameters of the theory in such a way that they absorb the quantities R and R', which depend on the range of force (see Ref. [55] for further details). The new renormalized parameters E_f and g_f are introduced as

$$[E_f - E_0]R_V + f_0^{\,2}[RR_V - R'^2] = 0\,, \tag{49}$$

$$g_f = 8\pi^2\mu\,\frac{E_f - E_{\mathrm{C}}}{R_V} = \frac{8\pi^2\mu f_0^2}{R_V^2}\,(R - R_V)^2. \tag{50}$$

In terms of the renormalized quantities, the t-matrix is given by

$$t(E) = \frac{1}{(2\pi)^2\mu}\,\frac{g_f}{2\mathcal{D}(E)}\,, \tag{51}$$

where

$$\mathcal{D}(E) = E - E_f - \frac{(E - E_f)^2}{E - E_{\mathrm{C}}} + \frac{\mathrm{i}}{2}\,g_f k\,. \tag{52}$$

Equation (51) resembles a well-known Flatté formula [59] for the near-threshold scattering amplitude and, if $|E_{\mathrm{C}}| \gg |E_f|$, we indeed arrive at the standard Flatté distribution

$$t(E) \underset{|E_{\mathrm{C}}| \gg |E_f|}{\approx} \frac{1}{(2\pi)^2\mu}\,\frac{(1/2)g_f}{E - E_f + (\mathrm{i}/2)g_f k}\,. \tag{53}$$

To establish a connection to Weinberg's work [38–40], we assume the existence of a near-threshold bound state with a binding energy E_{b}. In the vicinity of the bound-state pole, we then have

$$t(E) \simeq \frac{g^2_{\mathrm{eff}}}{E + E_{\mathrm{b}}}\,, \tag{54}$$

where (see Refs [38–40])

$$g^2_{\mathrm{eff}} = \frac{\sqrt{2\mu E_{\mathrm{b}}}}{4\pi^2\mu^2}(1 - Z)\,, \tag{55}$$

and the quantity Z is defined by the relation

$$\frac{Z}{1 - Z} = \frac{2E_{\mathrm{b}}}{E_{\mathrm{b}} + E_{\mathrm{C}}}\left(1 - \frac{\gamma_V}{\sqrt{2\mu E_{\mathrm{b}}}}\right). \tag{56}$$

We note that for $Z = 0$, expression (55) turns into the standard formula that defines the coupling constant of a compound object in terms of the binding energy of its constituents [60].

The zero of the elastic scattering amplitude is located at

$$E_{\rm C} = -E_{\rm b}\left(1 - \frac{2(1-Z)}{Z} + \frac{2(1-Z)}{Z}\,\frac{\gamma_V}{\sqrt{2\mu E_{\rm b}}}\right). \qquad (57)$$

Finally, for the scattering phase δ in the mesonic channel we can find

$$k\cot\delta = -\sqrt{2\mu E_{\rm b}} + \frac{\sqrt{2\mu E_{\rm b}}(E+E_{\rm b})(E_{\rm b}+E_{\rm C})}{2E_{\rm b}(E-E_{\rm C})}\,\frac{Z}{1-Z}\,. \qquad (58)$$

Generally, because of the aforementioned zero of the scattering amplitude, Eqn (58) does not allow an effective-range expansion. This expansion is recovered only if $|E_{\rm C}| \gg E_{\rm b}$, and then the most famous Weinberg formulas for the scattering length a and the effective radius $r_{\rm e}$ arise:

$$a = \frac{2(1-Z)}{2-Z}\,\frac{1}{\sqrt{2\mu E_{\rm b}}}\,, \qquad (59)$$

$$r_{\rm e} = -\frac{Z}{1-Z}\,\frac{1}{\sqrt{2\mu E_{\rm b}}} + O\left(\frac{1}{\beta}\right). \qquad (60)$$

Thus, if the effective-range expansion exists, we have a powerful tool at our disposal, which allows us to distinguish compact (elementary) bound states from molecular (composite) ones. Indeed, if $Z \approx 1$ and therefore the state is elementary, the effective range in Eqn (60) is large and negative, and the scattering length is small [see Eqn (59)]. If, on the contrary, the state is molecular ($Z \ll 1$), the situation is the opposite: the effective range is small (it can be positive if the range-of-force corrections are taken into account), and the scattering length is large.

Complementary to the Weinberg formulas is the 'pole counting' procedure [61]. Rewriting the denominator in Flatté formula (53) in terms of the effective-range parameters with

$$a = -\frac{g_f}{2E_f}\,, \qquad r_{\rm e} = -\frac{2}{\mu g_f}\,, \qquad (61)$$

we find the t-matrix poles

$$k_{1,2} = \frac{\rm i}{r_{\rm e}} \pm \sqrt{-\frac{1}{r_{\rm e}^2} + \frac{2}{a r_{\rm e}}}\,. \qquad (62)$$

If there is a bound state, the pole positions are given by

$$k_1 = {\rm i}\sqrt{2\mu E_{\rm b}}\,, \qquad k_2 = -{\rm i}\,\frac{2-Z}{Z}\,\sqrt{2\mu E_{\rm b}}\,, \qquad (63)$$

and therefore the first pole is on the physical sheet, while the second is on the unphysical sheet. If $Z \approx 1$ (elementary state), then the effective coupling g_f is small, while the effective range $r_{\rm e} \to -\infty$, and hence there are two almost symmetric near-threshold poles. If $Z \ll 1$ (molecular state), then the coupling g_f is large, the effective range is small, and hence there is only one near-threshold pole.

If there is no bound state in the system (the scattering length is negative), the pole counting procedure also works. If the coupling g_f is small, then $r_{\rm e} \to -\infty$ and $k_{1,2} \to \pm\sqrt{2\mu E_f}$, and therefore there are two near-threshold poles, which corresponds to the resonance case. For larger values of g_f, the poles move deeper into the complex plane and eventually collide on the imaginary axis. If the coupling is very large, the effective range is small, and there is only one near-threshold pole, which corresponds to a virtual state. One might argue that the probabilistic interpretation is lost in the case of a resonance/virtual state. This is not the case, however. In the low-energy approximation, spectral density (42) (which defines the probability of finding a bare state in the continuum) is expressed in terms of Flatté parameters as

$$w(E) = \frac{1}{2\pi}\,\frac{g_f k}{\left|E - E_f + ({\rm i}/2)g_f k\right|^2}\,. \qquad (64)$$

This, together with normalization condition (43) for the spectral density, allows drawing conclusions on the relative weight of the molecular component in the wave function of the state: we simply integrate expression (64) over the near-threshold region (see [53] for further details).

Weinberg's formulas look transparent when there is no near-threshold t-matrix zero. To understand what happens in the general case, it is instructive to study the singularities of the amplitude in terms of the variables E_f, g_f, and γ_V. Because

$$E_{\rm C} = E_f - \frac{1}{2}\,g_f\gamma_V\,, \qquad (65)$$

the expression for the t-matrix in Eqn (51) can be rewritten in the form

$$t(E) = \frac{1}{4\pi^2\mu}\,\frac{E - E_f + (1/2)g_f\gamma_V}{(E-E_f)(\gamma_V - {\rm i}k) + ({\rm i}/2)g_f\gamma_V k}\,, \qquad (66)$$

which shows that the t-matrix can have up to three near-threshold poles. A detailed analysis [55] of these singularities shows that the appearance of a t-matrix zero corresponds to the case of all three poles residing near the threshold. This requires (i) the direct interaction in the mesonic channel to be strong enough to support a bound or virtual state and (ii) a near-threshold bare quark state to exist, with a weak coupling to the mesonic channel. In other words, the pole generated by direct interaction collides with the pair of poles corresponding to the bare state, and this collision results in a breakdown of the effective-range expansion.

If at least one of the conditions above is not satisfied, there is no t-matrix zero in the near-threshold region, the effective-range formulas are valid, and the conclusions in Refs [40, 53, 61] hold: a large and negative effective range corresponds to a compact quark state, while a small effective range implies that the state is composite. In the former case, there are two near-threshold poles in the t-matrix, while in the latter case, there is only one pole.

In the double-pole situation, we can definitively state that the resonance is generated by an s-channel exchange, with a small coupling of this quark state to the mesonic continuum. In the single-pole situation, no model-independent insight into the underlying dynamics is possible, and we can only conclude that the resonance is generated dynamically.

A final comment is in order here. We consider the case of a bound state and no direct interaction in the mesonic channel. It is straightforward to derive a formula that expresses the Z factor through the binding energy and the 'bare' coupling constant between the channels f_0 [see the definition in Eqn (46)],

$$\frac{1}{Z} - 1 \approx \frac{4\pi^2\mu^2 f_0^2}{\sqrt{2\mu E_{\rm b}}}\,. \qquad (67)$$

It follows from formula (67) that for a decreasing binding energy, the Z factor also decreases, thus approaching zero as $Z \propto \sqrt{E_b}$ in the limit $E_b \to 0$. In other words, the closer the resonance resides to the threshold, the larger is the contribution of the molecular component to its wave function, that is, the more 'compound' it becomes. Furthermore, even a tiny 'bare' coupling f_0 of the quark channel to the mesonic channel is sufficient to reach any large (close to unity) value of the 'molecularness' (i.e., the value of $1 - Z$) of the physical state due to its proximity to the threshold. Such a conclusion is quite natural given that the proximity of the resonance to a threshold facilitates its transition to the corresponding final state, and therefore the probability of observing the resonance in the given hadronic channel is enhanced, which by definition increases the 'molecularness' of this near-threshold resonance.

It is also important that the Weinberg approach is model-independent. The Z factor defines the residue of the t-matrix (and therefore that of the amplitude) at the bound state pole: see Eqns (54) and (55). Because the probability evaluated from this amplitude is an observable quantity, all the parameters entering it are model- and scheme-independent. This way, for a given binding energy E_b, the value of the Z factor is defined uniquely and in a model-independent way.

Furthermore, deeper reasons for the model-independence of the Z factor can be identified. In the approach of effective field theories, parameters entering the Lagrangian are subject to renormalization and as such can be model-dependent (in the sense of the dependence on the regularization scheme). But such a renormalization is done by adding counter terms to the Lagrangian with only an analytic dependence on the energy allowed. This implies that the terms proportional to $\sqrt{E}$ cannot be affected by renormalization and are fixed in a model-independent way. This square-root behavior is typical for the key quantities in the Weinberg approach, in particular, the Z factor. Thus, as long as the binding energy is small enough for the binding momentum $\gamma = \sqrt{2\mu E_b}$ to be small compared to the inverse range of force β, the long-range part of the wave function of such a resonance is model-independent and totally defined by the value of γ.

3.3 Interplay of quark and meson degrees of freedom: two-channel case

Of particular relevance for X(3872) is the case of two nearby S-wave thresholds, $D^0\bar{D}^{*0}$ and D^+D^{*-}, split by $\Delta = M_{th_2} - M_{th_1} \approx 8$ MeV, such that the physical state X is a mixture of a bare-quark state and two mesonic components,

$$|X\rangle = \begin{pmatrix} c|\psi_0\rangle \\ \chi_1(\mathbf{p})|M_{11}M_{12}\rangle \\ \chi_2(\mathbf{p})|M_{21}M_{22}\rangle \end{pmatrix}. \tag{68}$$

Here, the subscripts 1 and 2 denote the respective $D^0\bar{D}^{*0}$ and D^+D^{*-} components.

We assume in what follows that the bare state is an isosinglet and set $f_1(\mathbf{p}) = f_2(\mathbf{p}) \equiv f(\mathbf{p})/\sqrt{2}$ in all general formulas, where the factor $1/\sqrt{2}$ is introduced for convenience of comparing with the single-channel case. The low-energy reduction and renormalization procedure are performed in a way quite similar to the one described in Section 3.2. In particular, as the first step, we define the t-matrix for the direct potential V and parameterize it in the scattering length approximation

$$t^V = \frac{1}{4\pi^2\mu\,\mathrm{Det}} \begin{pmatrix} \frac{1}{2}(\gamma_s + \gamma_t) + ik_2 & \frac{1}{2}(\gamma_t - \gamma_s) \\ \frac{1}{2}(\gamma_t - \gamma_s) & \frac{1}{2}(\gamma_s + \gamma_t) + ik_1 \end{pmatrix}, \tag{69}$$

where

$$\mathrm{Det} = \gamma_s\gamma_t - k_1k_2 + \frac{i}{2}(\gamma_s + \gamma_t)(k_1 + k_2)\,, \tag{70}$$

the quantities γ_s and γ_t are the inverse scattering lengths in the isospin-singlet and triplet channels,

$$k_1 = \sqrt{2\mu E}\,, \qquad k_2 = \sqrt{2\mu(E - \Delta)}\,, \tag{71}$$

and μ is the reduced mass (because the splitting Δ is small compared to the masses of the mesons, the reduced masses in the charged and neutral channel are set equal to each other).

Then, setting

$$E_f = E_0 - \frac{f_0^2}{R_s}(RR_s - R'^2)\,, \tag{72}$$

$$E_C = E_0 - f_0^2(R_s + R - 2R')\,, \tag{73}$$

$$g_f = \frac{8\pi^2\mu}{R_s^2}\, f_0^2(R_s - R')^2\,, \tag{74}$$

where $R_s = 4\pi^2\mu\gamma_s$, we readily arrive at the expression for the full mesonic t-matrix

$$t_{11} = \frac{1}{8\pi^2\mu}\,\frac{\gamma_s(E - E_f) + (E - E_C)(\gamma_t + 2ik_2)}{D(E)}\,, \tag{75}$$

$$t_{12} = t_{21} = \frac{1}{8\pi^2\mu}\,\frac{\gamma_t(E - E_C) - \gamma_s(E - E_f)}{D(E)}\,, \tag{76}$$

$$t_{22} = \frac{1}{8\pi^2\mu}\,\frac{\gamma_s(E - E_f) + (E - E_C)(\gamma_t + 2ik_1)}{D(E)}\,, \tag{77}$$

where

$$D(E) = \gamma_s\left[\gamma_t + \frac{i}{2}(k_1 + k_2)\right](E - E_f) - \left[k_1k_2 - \frac{i}{2}\gamma_t(k_1 + k_2)\right](E - E_C)\,. \tag{78}$$

Expressions (75)–(77) were derived in Ref. [56]. An alternative derivation of these expressions can be found in Ref. [62].

It is easy to demonstrate that the isosinglet element of the t-matrix has a zero at $E = E_C$. Similarly to the single-channel case [see Eqn (65)], the coupling constant g_f and the parameter E_C are related as

$$E_C = E_f - \frac{1}{2}\,g_f\gamma_s\,, \tag{79}$$

and therefore the zero at E_C is generated in the near-threshold region if the condition $|\gamma_s| \lesssim \Delta/g_f$ holds; otherwise, it leaves the region of interest.

Another phenomenon that affects the observables is momentum entanglement: the momenta k_1 and k_2 enter the expressions for the t-matrix in a complicated nonlinear way, including the product k_1k_2 [see also Ref. [63] for a discussion of the related effect on the line shapes for X(3872)]. This entanglement of mesonic channels is

governed by the triplet inverse scattering length γ_t and becomes strong for $|\gamma_t| \lesssim \sqrt{\mu\Delta}$.

In such a way, we can identify the following limit cases:
(i) $|\gamma_s| \to \infty$ and $|\gamma_t| \to \infty$.
(ii) small γ_s and $|\gamma_t| \to \infty$.
(iii) $|\gamma_s| \to \infty$ and small γ_t.
(iv) both γ_s and γ_t are small.

Case (i) corresponds to a weak direct interaction and is described by the two-channel Flatté formula with the denominator containing a plain sum of the contributions from the two channels, $g_f(k_1 + k_2)/2$. For a small coupling g_f, we have $Z \to 1$, and the state is mostly compact, while a large g_f corresponds to $Z \to 0$, and the state is predominantly molecular.

Case (ii) is effectively a single-channel one: with $|\gamma_t| \to \infty$, interaction in the isotriplet channel is weak, channel entanglement is irrelevant, the interplay between the quark and mesonic degrees of freedom occurs in the isosinglet channel, and the dynamics are defined by the t-matrix zero.

In contrast, case (iii) is free from the t-matrix zero, and the dynamics are defined by the channel entanglement, which is in turn governed by the isotriplet scattering length.

Case (iv) is a generic case, where all the aforementioned effects play a role for the dynamics of the system.

Because there is no hope that any data on the $D^{(*)}$-meson scattering could become available, our knowledge comes from studies of resonance production in various reactions. Therefore, we consider production line shapes (production differential rates) of a given resonance under various assumptions concerning its production mechanism. In particular, we study the production of neutral $D^0\bar{D}^{*0}$ mesons through the hadronic and quark component. The corresponding amplitudes are obtained by a low-energy reduction of general formulas (44) and (45). We assume that the t-matrix has a near-threshold pole, which allows us to ignore the Born terms in the production via the hadronic components [the first term in the right-hand side in Eqn (44)]; a detailed discussion of this issue can be found in Ref. [55].

If we disregard interference among the three possible production mechanisms, it is straightforward to find the corresponding differential branchings

$$\frac{\mathrm{d}\,\mathrm{Br}_q}{\mathrm{d}E} = \Theta(E)\,\frac{\mathcal{B}_0\sqrt{E}}{|D(E)|^2}\,\gamma_s{}^2|\gamma_t + \mathrm{i}k_2|^2\,, \tag{80}$$

$$\frac{\mathrm{d}\,\mathrm{Br}_{h_1}}{\mathrm{d}E} = \Theta(E)\,\frac{\mathcal{B}_1\sqrt{E}}{|D(E)|^2}\left|\gamma_s(E - E_f) + (\gamma_t + 2\mathrm{i}k_2)\left(E - E_f + \frac{1}{2}\,g_f\gamma_s\right)\right|^2, \tag{81}$$

$$\frac{\mathrm{d}\,\mathrm{Br}_{h_2}}{\mathrm{d}E} = \Theta(E)\,\frac{\mathcal{B}_2\sqrt{E}}{|D(E)|^2}\left|\gamma_s(E - E_f) - \gamma_t\left(E - E_f + \frac{1}{2}\,g_f\gamma_s\right)\right|^2, \tag{82}$$

where the denominator $D(E)$ is given by Eqn (78). The coefficients $\mathcal{B}_0$, $\mathcal{B}_1$, and $\mathcal{B}_2$ only define the overall normalization of the distributions.

In [56], examples of line shapes are given corresponding to all four cases (i)–(iv). For definiteness, the parameters of the problem were fixed as

$$\mu = 966.5\ \mathrm{MeV}\,, \qquad \Delta = 8.1\ \mathrm{MeV}\,, \qquad g_f = 0.25\,, \tag{83}$$

Table 1. Scattering length parameters, the Flatté parameter E_f, and the Z factor for the bound state with $E_b = 0.5$ MeV for cases (i)–(iv).

Case	γ_s, MeV	γ_t, MeV	E_f, MeV	Line	Z
(i)	$\pm\infty$	$\pm\infty$	−10.47	Solid	0.30
(ii)	−30	$\pm\infty$	−3.22	Dashed	0.85
(iii)	$\pm\infty$	−30	−7.77	Dashed-dotted	0.19
(iv)	−30	−30	−2.97	Dotted	0.67

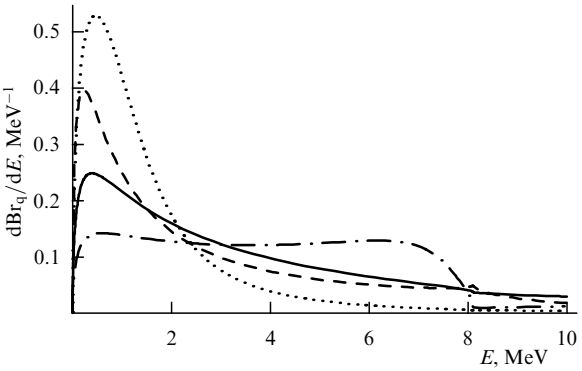

Figure 3. Differential production rate through the quark component (80). Cases (i)–(iv) are given by the respective solid, dashed, dashed-dotted, and dotted lines. Adapted from Ref. [56].

and the values of γ_s, γ_t, and E_f are listed in Table 1. For each case above, the Flatté parameter E_f was tuned to provide a bound state with $E_b = 0.5$ MeV.

In Figs 3–5, we plot the line shapes for X production via the quark component and both mesonic components for all four cases (i)–(iv). For each individual curve in Figs 3–5, the integral over the near-threshold region (chosen to be from 0 to 10 MeV) equals unity (in units of MeV^{-1}), which fixes the overall normalization factors $\mathcal{B}_0$, $\mathcal{B}_1$, and $\mathcal{B}_2$.

As can be seen from the examples above, the interplay of various degrees of freedom gives rise to a highly complicated resonance line shape. If experimental data display such phenomena, we can conclude that the resonance is generated by complicated nontrivial dynamics. The converse is, generally speaking, not correct: due to the interference between production mechanisms, the resulting near-threshold line shape could be smooth enough even in the presence of the competing quark and meson dynamics. This, however, requires a suitable fine-tuning of the production parameters, which seems very implausible.

4. Microscopic quark model for X(3872)

As was already mentioned in the Introduction, the $\bar{c}c$ assignment for X(3872) seems to be ruled out by its mass: the state is too low to be a 2^3P_1 charmonium. However, a possibility exists that a strong coupling to $D^{(*)}$ pairs could distort the bare $\bar{c}c$ spectrum. In this section, we address the question of whether such a possibility can be realized in the existing quark models. For this, the general formalism presented in Section 3.1 is used.

As a prerequisite, the transition form factors that describe the coupling of D-meson pairs to the bare $\bar{c}c$ charmonium must be calculated. This requires a model for light-quark pair creation. The simplest model of such a kind is the so-called $^3P_0$ model suggested many years ago in Ref. [64]. It assumes that the light-quark pair is created uniformly in space with the

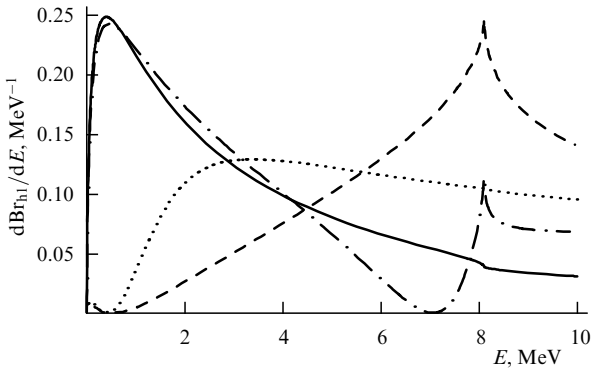

Figure 4. Differential production rate via the first mesonic component, Eqn (81). Cases (i)–(iv) are given by the respective solid, dashed, dashed-dotted, and dotted lines. Adapted from Ref. [56].

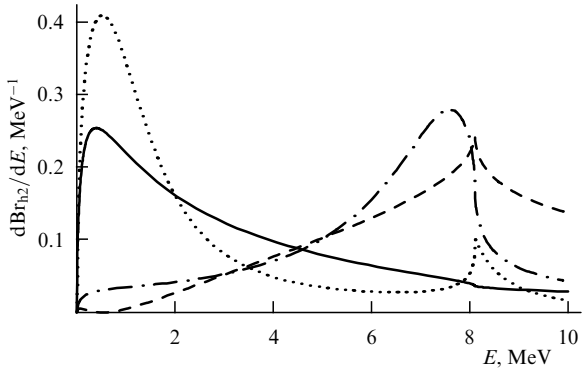

Figure 5. Differential production rate via the second mesonic component (82). Cases (i)–(iv) are given by the respective solid, dashed, dashed-dotted, and dotted lines. Adapted from Ref. [56].

vacuum quantum numbers 0^{++}, which means that this is a $^3\mathrm{P}_0$ pair, hence the name of the model. Applications of this purely phenomenological model have a long history (see, e.g., Refs [65–67] and more recent developments in Refs [21, 68]).

More sophisticated models for the pair-creation operator also exist, where the current–current interaction is constructed using the confining force and one-gluon exchange. Examples of such calculations can be found in the Cornell model [1], which assumes that confinement has a Lorentz vector nature. The model used in Ref. [69] assumes that the confining interaction is scalar. Possible mechanisms of strong decays were studied in the framework of the Field Correlator Method (FCM) (see, e.g., review [70]), and an effective $^3\mathrm{P}_0$ operator for the pair creation emerged from this study, with the coupling computed in terms of the FCM parameters [71]. For the purposes of this review, it is sufficient to stick to the generic version of the $^3\mathrm{P}_0$ model to calculate the transition form factors. Further details of the approach can be found in Ref. [72].

It is assumed in the model that the pair-creation Hamiltonian for a given quark flavor q is a nonrelativistic reduction of the expression

$$H_\mathrm{q} = g_\mathrm{q} \int \mathrm{d}^3x\, \bar{\psi}_\mathrm{q}\psi_\mathrm{q}\,, \tag{84}$$

and hence the spatial part of the amplitude of the decay $A \to B + C$ of the initial meson A in the center-of-mass frame is given by the operator

$$\hat{f}(\mathbf{p}) = \int \mathrm{d}^3k\, \phi_A(\mathbf{k}-\mathbf{p})\hat{O}(\mathbf{k})\phi_B^*(\mathbf{k}-r_\mathrm{q}\mathbf{p})\phi_C^*(\mathbf{k}-r_\mathrm{q}\mathbf{p})\,,$$
$$r_\mathrm{q} = \frac{m_\mathrm{q}}{m_\mathrm{q}+m_\mathrm{c}}\,, \tag{85}$$

where ϕ_A is the wave function of the initial meson in momentum space, ϕ_B and ϕ_C are those of the final mesons B and C, $\mathbf{p} = \mathbf{p}_B = -\mathbf{p}_C$, and m_c and m_q are the charmed and light quark masses. The $^3\mathrm{P}_0$ pair creation operator is taken in the form

$$\hat{O}(\mathbf{k}) = -2\gamma\boldsymbol{\sigma}\mathbf{k}\,, \qquad \gamma = \frac{g_\mathrm{q}}{2m_\mathrm{q}}\,, \tag{86}$$

and the matrix $\boldsymbol{\sigma}$ acts on the spin variables of the light quark and antiquark (heavy quarks are treated as spectators). To arrive at the vertex $f_i(\mathbf{p})$ for a particular mesonic channel i, which enters equations in Section 3.1, the matrix element of the operator $\hat{f}(\mathbf{p})$ must be evaluated between the spin wave functions of the initial and final states.

The behavior of form factors (85) is determined by the scales of the wave functions involved, which are in turn determined by the quark model. In the standard nonrelativistic potential model, the Hamiltonian is

$$H_0 = \frac{p^2}{m_\mathrm{c}} + V(r) + C\,, \qquad V(r) = \sigma r - \frac{4}{3}\frac{\alpha_\mathrm{s}}{r}\,, \tag{87}$$

where σ is the string tension, α_s is the strong coupling constant, and the constant C defines an overall shift of the spectrum. Hamiltonian (87) must be supplied with Fermi–Breit-type relativistic corrections including the spin–spin, spin–orbit, and tensor forces, which cause splittings in the $^{2S+1}L_J$ multiplets. In the leading approximation, these splittings should be calculated as perturbations averaged over the eigenfunctions of Hamiltonian (87). The same interaction $V(r)$ is used in calculations of the spectra and wave functions of D mesons.

In the calculations in Ref. [72], the coupled-channel scheme of Section 3.1 was used, with the direct interaction in the mesonic channels disregarded. The decay channels participating in the coupled-channel scheme were chosen to be $\mathrm{D\bar{D}}$, $\mathrm{D\bar{D}^*}$, $\mathrm{D^*\bar{D}^*}$, $\mathrm{D_s\bar{D}_s}$, $\mathrm{D_s\bar{D}_s^*}$, and $\mathrm{D_s^*\bar{D}_s^*}$, and the mass difference between the charged and neutral charmed mesons was not taken into account. The parameters of the underlying quark model and the pair-creation strength γ were chosen to reproduce, with a reasonable accuracy, the masses of the 1S, 1P, and 2S charmonium, as well as the mass and the width of the $^3\mathrm{D}_1$ $\psi(3770)$ state.

The masses of the charmonia lying below the open-charm threshold are given by the poles of the t-matrix [see Eqns (33)–(37)]: they are solutions of the equation

$$M - M_0 + \mathcal{G}(M) = 0\,, \quad \mathcal{G}(M) = \sum_i \int f_i^2(\mathbf{q})S_i(\mathbf{q})\,\mathrm{d}^3q\,, \tag{88}$$

where M is the physical mass and M_0 is the bare mass evaluated in potential model (87) with the Fermi–Breit corrections taken into account. As regards the above-threshold state $\psi(3770)$, its 'visible' mass M_R was defined from the equation

$$M_\mathrm{R} - M_0 + \mathrm{Re}\,\mathcal{G}(M_\mathrm{R}) = 0\,, \tag{89}$$

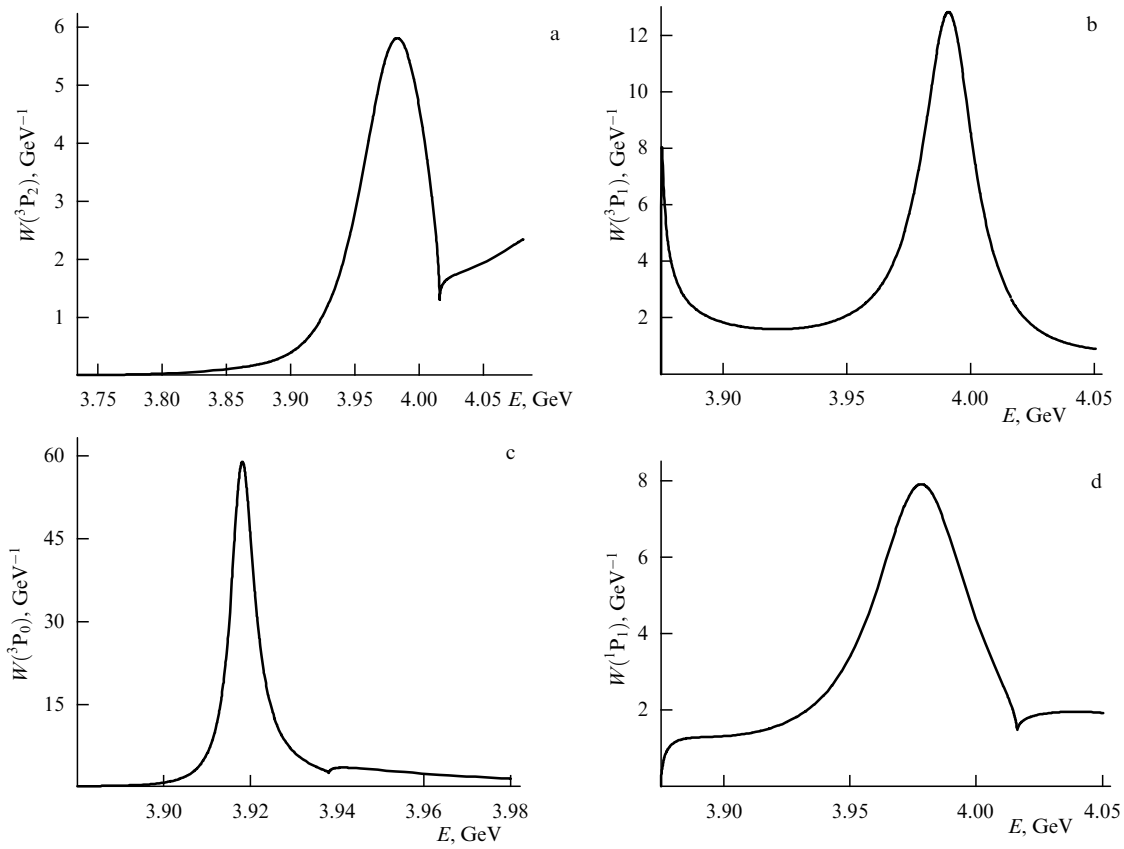

Figure 6. Spectral density of the bare 2P states. (Adapted from Ref. [72].)

and its 'visible' width was computed as

$$\Gamma = 2\Re \operatorname{Im} \mathcal{G}(M_{\mathrm{R}}), \quad \Re = \left(1 + \frac{\partial \operatorname{Re} \mathcal{G}(M)}{\partial M}\bigg|_{M=M_{\mathrm{R}}}\right)^{-1}. \quad (90)$$

Hadronic shifts (the difference between the bare mass M_0 and the physical mass M) for lower-lying charmonia were calculated to be of the order of 200 MeV, and Z factors range from ≈ 0.9 for the 1S states to $\approx 0.75-0.8$ for 2S ones. In other words, although the coupled-channel effects are substantial, the resulting spectra are not changed beyond recognition.

The situation with the 2P levels promises more, because 2P charmonia are expected to populate the mass range 3.90–4.00 GeV, where more charmed meson channels start to open, and some of these channels are S-wave ones.

The visible masses and widths of the 2P states were also calculated with the help of Eqns (89) and (90); the results are given in Table 2. At first glance, nothing dramatic has happened due to the S-wave thresholds. Indeed, similarly to the S-wave charmonia, the bare P-wave states suffer from hadronic shifts, but these are not too large, about 200 MeV, and the states acquire rather moderate finite widths. To reveal the role of the S-wave thresholds, the spectral density of the bare states, which is depicted in Fig. 6, must be studied. In addition to clean and rather narrow Breit–Wigner resonances in all considered channels, we then observe a near-threshold peak in the 1^{++} channel (and only in this channel!) rising against a flat background.[2]

Table 2. Masses and widths (in units of MeV) of the 2P charmonium states evaluated in Ref. [72] in the framework of a potential quark model.

J^{PC}	Bare mass, MeV	Physical mass, MeV	Width, MeV
1^{+-}	4200	3980	50
2^{++}	4230	3990	68
1^{++}	4180	3990	27
0^{++}	4108	3918	7

The elastic $D\bar{D}^*$ scattering length in the 1^{++} channel turns out to be negative and large,

$$a_{D\bar{D}^*} = -8 \text{ fm}, \quad (91)$$

signaling the presence of a virtual state very close to the $D\bar{D}^*$ threshold (with the energy of just 0.32 MeV relative to it). By slightly decreasing the value of the bare mass and/or increasing the value of the pair-creation strength γ, we can shift the virtual state closer to the threshold and eventually move the pole to the physical sheet, thus forming a bound state. Clearly, this near-threshold peak should be identified with X(3872). We note that in a more sophisticated version of the coupled-channel approach [73, 74], where the mass difference between the neutral and charged $D\bar{D}^*$ thresholds was taken into account, the X(3872) peak persists and resides at the neutral $D^0\bar{D}^{*0}$ threshold.

[2] There is an interesting possibility, discussed in Ref. [72], of an exotic line shape in the 0^{++} channel if the bare 2^3P_0 mass is shifted about 30 MeV upwards (which is not ruled out by the quark model because the uncertainty in the spin–orbit splitting is large for a scalar). In such a scenario, the physical 0^{++} state becomes about 3.94 GeV, that is, just at the $D_s\bar{D}_s$ threshold. Because of this threshold proximity, the line shape is severely non-Breit–Wigner, and a large admixture of the $D_s\bar{D}_s$ molecule is expected in the wave function of the state.

Thus, the coupling to the mesonic channels generates not only a resonance but also a bound/virtual state very close to the threshold. In fact, in the presented dynamical scheme, the X(3872) pole is an example of the so-called CC (coupled-channel) pole (see Ref. [75]): in the strong-coupling limit, an extra pole can come from infinity and move to the near-threshold region.

A natural question arises as to what extent this result is reliable. It was obtained in a naive nonrelativistic model whose relevance for light quarks is questionable. The applicability of the nonrelativistic coupled-channel formalism described in Section 3.1 and used here depends on whether the motion of the D-meson pairs can be treated as nonrelativistic in the considered energy range. Evaluating the transition vertices $f_i(\mathbf{p})$ is an essentially relativistic problem; however, the gross features of vertices (85) are quite general. First, at small ps, the vertex function behaves like p^{2l+1}, where l is the angular momentum in the D-meson system. Second, it decreases at large ps, and its falloff is determined by the overlap of the initial- and final-state wave function. The first feature above defines the analytic properties of the self-energy $\mathcal{G}(\mathcal{M})$, while the large-momentum behavior of the $f_i(\mathbf{p})$ is responsible, together with the effective coupling constant, for the hadronic shift of the bare state [we note here that the value of the effective coupling constant can be extracted from the experimental width of the $\psi(3770)$ state]. We therefore expect that the suggested coupled-channel scheme for the charmonium levels does not change qualitatively if more rigorous approaches are used, and resort to the $^3\mathrm{P}_0$ model as a simple illustration of a possible scenario of the X(3872) binding.

Another question to be asked is why it is not possible to generate CC states in other S-wave $\mathrm{D}^{(*)}\bar{\mathrm{D}}^{(*)}$ channels. One could naively assume that the heavy-quark limit requires this. Indeed, the heavy-quark limit implies that the initial states are degenerate in mass within a given $\{NL\}$ multiplet (here, N is the radial quantum number and L is the quark–antiquark orbital angular momentum) and have the same wave functions. The final two-meson states exhibit the same degeneracy. So-called loop theorems [76] demonstrate that in the heavy-quark limit, the total strong open-flavor widths are the same within a given $\{NL\}$ multiplet. As a consequence, the hadronic shift for a bare $\mathrm{Q}\bar{\mathrm{Q}}$ state is the same for all members of this multiplet.

Thus, in accordance with the loop theorems [76], the existence of the 1^{++} $\mathrm{D}\bar{\mathrm{D}}^*$ molecule would imply the existence of other molecules with the mesonic content given by the S-wave spin-recoupling coefficients of the P-wave levels of charmonium[3]:

$$\begin{aligned} 0^{++} &\to \frac{\sqrt{3}}{2}\,\mathrm{D}\bar{\mathrm{D}} + \frac{1}{2}\,\mathrm{D}^*\bar{\mathrm{D}}^*\,, \\ 1^{++} &\to \frac{1}{\sqrt{2}}(\mathrm{D}\bar{\mathrm{D}}^* + \bar{\mathrm{D}}\mathrm{D}^*)\,, \\ 1^{+-} &\to -\frac{1}{2}(\mathrm{D}\bar{\mathrm{D}}^* - \bar{\mathrm{D}}\mathrm{D}^*) + \frac{1}{\sqrt{2}}\,\mathrm{D}^*\bar{\mathrm{D}}^*\,, \\ 2^{++} &\to \mathrm{D}^*\bar{\mathrm{D}}^*\,. \end{aligned} \tag{92}$$

But the loop theorems are actually violated by the spin-dependent interaction for both the initial ($\bar{\mathrm{c}}\mathrm{c}$) and final ($\mathrm{D}^{(*)}\bar{\mathrm{D}}^{(*)}$) states. Because the generation of a CC state is essentially a threshold phenomenon, this circumstance prevents generation of X(3872) siblings in the coupled-channel dynamical scheme.

Indeed, the effective coupling constants of a bare level of charmonium with different mesonic channels are proportional to the corresponding spin-recoupling coefficients, which make the only difference between them in the heavy-quark limit. As is seen from relations (92), the full S-wave strength of the $^3\mathrm{P}_1$ decay is concentrated in the single $\mathrm{D}\bar{\mathrm{D}}^*$ channel, while for the $^1\mathrm{P}_1$ and $^3\mathrm{P}_0$ decays, it is diluted between two channels with different thresholds. As a result, in the latter case, the coupling constant appears to be not strong enough to support a CC state: for example, the scattering length $\mathrm{D}\bar{\mathrm{D}}^*$ in the $^1P_1$ channel, $|a| \simeq 1$ fm, is much smaller than the value quoted in Eqn (91) for the $^3\mathrm{P}_1$ channel. The problem with the $^3\mathrm{P}_2$ channel is of a different nature: the $\mathrm{D}^*\bar{\mathrm{D}}^*$ threshold with a mass of about 4.016 GeV lies too high, ruling out a 2^{++} CC state. We therefore conclude that the 1^{++} molecular state is unique within the coupled-channel model.[4]

5. Nature of X(3872) from data

In this section, we discuss the nature of the charmonium-like state X(3872). Given the proximity of this resonance to a threshold, a considerable admixture of the $\mathrm{D}\bar{\mathrm{D}}^*$ component in its wave function is inevitable. Therefore, a realistic model for the description of X(3872) developed in the preceding section assumes that its wave function contains both a short-range part (which can be associated with a genuine $\bar{\mathrm{c}}\mathrm{c}$ charmonium) and a long-range part (defined by the molecular component $\mathrm{D}\bar{\mathrm{D}}^*$), and proximity to the threshold implies that the admixture of the latter component is not small.

We start from a qualitative phenomenological consideration that supports such a picture. The isospin breaking that follows from the approximately equal probabilities of X(3872) decays into the final states $\rho\mathrm{J}/\psi$ and $\omega\mathrm{J}/\psi$ finds a natural explanation in the framework of the molecular model as coming from the mass difference $\Delta \approx 8$ MeV between the charged and neutral thresholds $\mathrm{D}\bar{\mathrm{D}}^*$ (see Refs [30, 31]). Indeed, in the molecular picture, the transition from X(3872) to any final state can proceed via intermediate $\mathrm{D}\bar{\mathrm{D}}^*$ loops and, for different isospin states, contributions from the loops with charged (L_c) and neutral (L_0) D mesons come either in a sum or in a difference. In particular, for the ratio of the effective coupling constants of X(3872) to the final states $\rho\mathrm{J}/\psi$ and $\omega\mathrm{J}/\psi$, we can find

$$\frac{g_{\mathrm{X}\to\rho\mathrm{J}/\psi}}{g_{\mathrm{X}\to\omega\mathrm{J}/\psi}} \sim \left|\frac{L_0 - L_\mathrm{c}}{L_0 + L_\mathrm{c}}\right| \sim \frac{\sqrt{m_\mathrm{D}\Delta}}{\beta} \sim 0.1\,, \tag{93}$$

where m_D is the mass of the $\mathrm{D}^{(*)}$ meson and $\beta \simeq 1$ GeV sets a typical scale of the real part of the loop defined by the range

[3] These relations do not depend on the pair-creation model and only assume that the spin of the heavy-quark pair is conserved in the decay.

[4] This statement applies only to the coupled-channel model in this section, which has no direct interaction between the mesons. In most work on the molecular states in the spectrum of charmonium and bottomonium (see, e.g., Refs [77–85]), the problem of binding is solved by using a short-range direct interaction between the heavy $\mathrm{D}^{(*)}$ or $\mathrm{B}^{(*)}$ mesons, which is responsible for the formation of a near-threshold pole that typically resides on the first (physical) Riemann surface sheet and is therefore a bound state. A description of X(3872) in the framework of such an approach constitutes the subject of Section 6.3; a discussion of the spin partners of X(3872) can be found in Refs [83, 84, 86–88].

of force. If the strongly different phase spaces for the considered decays are taken into account, then relation (93) is sufficient to explain the experimental ratio (5). For a pure $\bar{c}c$ state, such a violation of the isospin symmetry would be very difficult, if not impossible, to explain because ratio (93) for a genuine charmonium turns out to be an order of magnitude smaller than for a molecule (see, e.g., the discussion in Ref. [16]).

On the other hand, as was already mentioned in the Introduction, X(3872) is produced in B-meson decays with the branching fraction similar to those for genuine charmonia [see, e.g., relation (11)], while this branching fraction was shown to be very small for a molecule [89]. Similarly, doubts were cast in Ref. [90] on the molecular assignment based on the reality of a copious production of the X(3872) at high energies in hadron colliders. Recently, this point has become a subject of lively discussions (see, e.g., Refs [91, 92]).

While the details of X(3872) prompt production in the molecular picture are still to be clarified, the inclusion of a nonmolecular seed could certainly be helpful in resolving this contradiction.

We now turn to a quantitative description of X(3872) based on the existing experimental data. In particular, in this section we present a simple but realistic parameterization for the line shape of X(3872) [93, 94] and demonstrate that it allows making certain conclusions on the nature of the X(3872) state.

The X(3872) production line shapes in B-meson decays do not exhibit irregularities in the near-threshold region. Therefore, these line shapes can be described by the simple Flatté formula [59], which can be derived naturally in the coupled-channel model that includes a molecular component and a bare charmonium. More explicitly, the physical system contains a bare pole associated with the genuine $\bar{c}c$ charmonium χ'_{c1} (a radially excited axial-vector $\bar{c}c$ state), two elastic channels [a charged and a neutral $D\bar{D}^*$ channel split by $\Delta = M(D^+D^{*-}) - M(D^0\bar{D}^{*0}) \approx 8$ MeV], and a set of inelastic channels. We note that the existing experimental data can be well described if the inelastic channels are taken into account through an effective width $\Gamma(E)$ [93],

$$\Gamma(E) = \Gamma_{\pi^+\pi^- J/\psi}(E) + \Gamma_{\pi^+\pi^-\pi^0 J/\psi}(E) + \Gamma_0\,, \tag{94}$$

$$\Gamma_{\pi^+\pi^- J/\psi}(E) = f_\rho \int_{2m_\pi}^{M-m_{J/\psi}} \frac{\mathrm{d}m}{2\pi} \frac{q(m)\Gamma_\rho}{(m-m_\rho)^2 + \Gamma_\rho^2/4}\,, \tag{95}$$

$$\Gamma_{\pi^+\pi^-\pi^0 J/\psi}(E) = f_\omega \int_{3m_\pi}^{M-m_{J/\psi}} \frac{\mathrm{d}m}{2\pi} \frac{q(m)\Gamma_\omega}{(m-m_\omega)^2 + \Gamma_\omega^2/4}\,, \tag{96}$$

where

$$q(m) = \sqrt{\frac{\left(M^2 - (m+m_{J/\psi})^2\right)\left(M^2 - (m-m_{J/\psi})^2\right)}{4M^2}}, \qquad M = M(D^0\bar{D}^{*0}) + E\,, \tag{97}$$

f_ρ and f_ω are the coupling constants, and m_ρ, m_ω and Γ_ρ, Γ_ω are the masses and the widths of the ρ and ω mesons [4].

The quantity Γ_0 describes an additional inelasticity, which is taken into account effectively. The short-range charmonium χ'_{c1} component of X(3872) is responsible for this contribution to the X(3872) decay modes. These are annihilation modes into light hadrons, a $\chi_{1c}(3515)\pi\pi$ mode, and radiative decay modes.[5] In other words, these are all the inelastic decay modes of X(3872) except the $\rho J/\psi$ and $\omega J/\psi$ modes, which are included explicitly because of their substantial energy dependence [see expressions (95) and (96)]. Then, taking the value of the total width for the ground-state axial-vector charmonium $\chi_{c1}(3515)$ equal to 0.84 ± 0.04 MeV [4], and an estimate for the total width of the χ'_{c1} made in the framework of a quark model and yielding 1.72 MeV [20], it is quite natural to assume that the parameter Γ_0 takes a value of about 1–2 MeV. Correlating this parameter with the upper bound (3) on the X(3872) width, we fix this parameter as

$$\Gamma_0 = 1\ \text{MeV}\,. \tag{98}$$

Therefore, for the denominator in the distribution for X(3872), we have

$$D(E) = \begin{cases} E - E_f - \dfrac{1}{2}(g_1\kappa_1 + g_2\kappa_2) + \dfrac{\mathrm{i}}{2}\Gamma(E), & E < 0\,, \\ E - E_f - \dfrac{1}{2}\,g_2\kappa_2 + \dfrac{\mathrm{i}}{2}\big(g_1 k_1 + \Gamma(E)\big), & 0 < E < \Delta\,, \\ E - E_f + \dfrac{\mathrm{i}}{2}\big(g_1 k_1 + g_2 k_2 + \Gamma(E)\big), & E > \Delta\,, \end{cases} \tag{99}$$

where

$$k_1 = \sqrt{2\mu_1 E}, \quad \kappa_1 = \sqrt{-2\mu_1 E}, \qquad k_2 = \sqrt{2\mu_2(E-\Delta)}, \quad \kappa_2 = \sqrt{2\mu_2(\Delta - E)},$$

and μ_1 and μ_2 are the reduced masses in the elastic channels. The energy is measured from the $D^0\bar{D}^{*0}$ threshold. We set $g_1 = g_2 = g$, which is a good approximation in the isospin symmetry limit.

In accordance with the discussion at the beginning of this section, we assume that X(3872) is produced in B-meson decays via the $\bar{c}c$ component. The short-range dynamics of the weak $B \to K$ transition are absorbed into the coefficient $\mathcal{B}$, and we estimate this quantity to be

$$\mathcal{B} \equiv \mathrm{Br}(B \to K\chi'_{c1}) = (3-6) \times 10^{-4}\,, \tag{100}$$

because it is reasonable to expect that χ'_{c1} is produced in $B \to K$ decays at a rate comparable to other similar charmonia. We note that there is a quark model prediction $\mathrm{Br}(B \to K\chi'_{c1}) = 2 \times 10^{-4}$ [95]; however, the model used is known to underestimate the production rate for χ_{c1} more than twofold.

It is now straightforward to find the differential production rates in the inelastic channels

$$\frac{\mathrm{d}\,\mathrm{Br}(B \to K\pi^+\pi^- J/\psi)}{\mathrm{d}E} = \mathcal{B}\,\frac{1}{2\pi}\,\frac{\Gamma_{\pi^+\pi^- J/\psi}(E)}{\left|D(E)\right|^2}\,, \tag{101}$$

$$\frac{\mathrm{d}\,\mathrm{Br}(B \to K\pi^+\pi^-\pi^0 J/\psi)}{\mathrm{d}E} = \mathcal{B}\,\frac{1}{2\pi}\,\frac{\Gamma_{\pi^+\pi^-\pi^0 J/\psi}(E)}{\left|D(E)\right|^2}\,. \tag{102}$$

As regards the elastic channels, we consider the D^{*0} meson to be unstable with the decay branching fractions to the final

[5] The assumption about the radiative modes being insensitive to the long-range component of the X(3872) wave function is confirmed by calculations discussed in Section 8 below.

states $D^0\pi^0$ and $D^0\gamma$ with the relative probabilities [4]

$$\mathrm{Br}(D^{*0} \to D^0\pi^0) = (61.9 \pm 2.9)\%\,, \tag{103}$$

$$\mathrm{Br}(D^{*0} \to D^0\gamma) = (38.1 \pm 2.9)\%\,, \tag{104}$$

whence for the final state $D^0\bar{D}^0\gamma$ we find

$$\frac{\mathrm{d}\,\mathrm{Br}(B \to K D^0\bar{D}^0\gamma)}{\mathrm{d}E} = 0.38\,\mathcal{B}\,\frac{1}{2\pi}\,\frac{gk_1}{\bigl|D(E)\bigr|^2}\,. \tag{105}$$

In the case of the $D^0\bar{D}^0\pi^0$ final state, we also take the signal–background interference into account, which is defined by two parameters, the constant strength c and the relative phase ϕ. The differential production rate in this channel then takes the form

$$\frac{\mathrm{d}\,\mathrm{Br}(B \to K D^0\bar{D}^0\pi^0)}{\mathrm{d}E} = 0.62\,\frac{k_1}{2\pi}\left[\left(\mathrm{Re}\,\frac{\sqrt{g\mathcal{B}}}{D(E)} + c\cos\phi\right)^2 + \left(\mathrm{Im}\,\frac{\sqrt{g\mathcal{B}}}{D(E)} + c\sin\phi\right)^2\right]. \tag{106}$$

The last ingredient needed for the data analysis is the spectral density, and it is easy to find the explicit expression for it:

$$w(E) = \frac{1}{2\pi\bigl|D(E)\bigr|^2}\bigl(gk_1\Theta(E) + gk_2\Theta(E-\Delta) + \Gamma(E)\bigr)\,. \tag{107}$$

In accordance with the approach outlined in Section 3.2, the integral of $w(E)$,

$$W = \int_{E_{\min}}^{E_{\max}} w(E)\,\mathrm{d}E\,, \tag{108}$$

taken over the near-threshold region defines the admixture of the genuine charmonium χ'_{c1} in the X(3872) wave function. For the problem under consideration, a natural definition of the near-threshold region is the energy interval $-10 \lesssim E \lesssim 10$ MeV, which covers the neutral three-body threshold at $E_{D^0\bar{D}^0\pi^0} \approx -7$ MeV and the charged two-body threshold at $E_{D^+\bar{D}^{*-}} \equiv \Delta \approx 8$ MeV.

Now, it is easy to estimate the total branching fraction for the X(3872) production as

$$\mathrm{Br}(B \to KX) = \mathcal{B}W < 2.6 \times 10^{-4}\,, \tag{109}$$

where experimental bound (4) was used.[6]

Finally, Table 3 contains estimates for the widths of the radiative decays of χ'_{c1} obtained in various quark models. They are used in what follows.

Thus, the X(3872) model is defined by a set of 8 parameters,

$$\Gamma_0\,,\quad g\,,\quad E_f\,,\quad f_\rho\,,\quad f_\omega\,,\quad \mathcal{B}\,,\quad \phi\,,\quad c\,, \tag{110}$$

and is to describe the X(3872) line shape in the energy interval near the neutral $D\bar{D}^*$ threshold.

[6] In [93, 94], a different upper bound $\mathrm{Br}(B \to KX) < 3.2 \times 10^{-4}$, relevant at that time, was used, which had been established by the BABAR Collaboration [96] in 2006. However, the results of the analysis performed are insensitive to a particular value of this bound.

Table 3. Some typical estimates for the radiative decay width of the charmonium χ'_{c1} obtained in various quark models.

$\Gamma(\chi'_{c1} \to \gamma J/\psi)$, keV	$\Gamma(\chi'_{c1} \to \gamma\psi')$, keV	R [see definition (16)]	Reference
11	64	5.8	[20]
70	180	2.6	[21]
50 – 70	50 – 60	0.8 ± 0.2	[97]
30.8 – 42.7	70.5 – 73.2	1.65 – 2.38	[98]

The data analyzed in this section come from the Belle Collaboration (see Ref. [10] for the $D^0\bar{D}^0\pi^0$ channel and Ref. [99] for the $\pi^+\pi^- J/\psi$ channel) and the BABAR Collaboration (see Ref. [11] for the combined $D^0\bar{D}^{*0}$ mode, which is a sum of the $D^0\bar{D}^0\pi^0$ and $D^0\bar{D}^0\gamma$ channels, and Ref. [100] for the $\pi^+\pi^- J/\psi$ channel). Parameters of the experimental distributions are listed in Table 4.

To be directly compared with the experimental distributions, the theoretical differential production rates must be convolved with the detector resolution function, which has the form of a Gaussian with the parameter σ quoted in Table 4 for all data sets.[7] Then the resulting differential production rates are to be converted to the number-of-events distributions by means of the relation

$$N(E) = E_{\mathrm{bin}}\left(\frac{N_{\mathrm{tot}}}{\mathrm{Br}_{\mathrm{tot}}}\right)\frac{\mathrm{d}\,\mathrm{Br}}{\mathrm{d}E}\,, \tag{111}$$

where N_{tot} is the total number of events, $\mathrm{Br}_{\mathrm{tot}}$ is the total branching, and E_{bin} is the bin size. All these parameters are listed in Table 4.

The procedure is to make a simultaneous fit for the data from the same collaboration on the $\pi^+\pi^- J/\psi$ and $D^0\bar{D}^{*0}$ channels. For each data set, two possibilities are considered: a bound state and a virtual level. These two situations are distinguishable by the sign of the real part of the $D^0\bar{D}^{*0}$ scattering length, for which the following formula can be easily obtained:

$$a = -\frac{1}{\sqrt{2\mu_2\Delta} + \bigl(2E_f - \mathrm{i}\Gamma(0)\bigr)/g}\,. \tag{112}$$

Several sets of parameters that yield the best description of the data are listed in Table 5. The name of each set indicates the collaboration whose data are processed and the type of description: bound state (b) or virtual level (v).[8] The scattering length is calculated in accordance with Eqn (112) and for the estimates of the width $\Gamma(\gamma\psi')$, the experimental relation $\mathrm{Br}(\gamma\psi') \simeq \mathrm{Br}(\pi^+\pi^- J/\psi)$ is used [see Eqn (14)].

The theoretical curves for the resonance line shapes for all four cases are shown in Fig. 7, together with the corresponding integrals over bins (black dots), in comparison with the experimental data (unfilled circles with error bars) [93, 94].

[7] Because the BABAR resolution function in the $D^0\bar{D}^{*0}$ channel takes a very complicated form and is not available in the public domain, in the present analysis we use a Gaussian function with the parameter $\sigma = 1$ MeV in the calculations.

[8] In view of the inelasticity present in the system, the X(3872) pole in the complex energy plane does not lie on the real axis and is somewhat shifted into the complex plane, such that, strictly speaking, it describes a resonance rather than a bound or virtual state. Nevertheless, it is convenient to stick to the notions of the bound and virtual levels defined for the Riemann surface for the elastic channels only.

Table 4. Parameters of the experimental distributions from Belle [10, 99] and BABAR [11, 100].

Collaboration	Channel	$N_{\rm tot}$	$\mathrm{Br}_{\rm tot}$	$E_{\rm bin}$, MeV	σ, MeV
Belle	$\pi^+\pi^-\mathrm{J}/\psi$	131	8.3×10^{-6}	2.5	3
Belle	$\mathrm{D}^0\bar{\mathrm{D}}^0\pi^0$	48.3	0.73×10^{-4}	2.0	$0.172\sqrt{m-M(\mathrm{D}\bar{\mathrm{D}}^*)}$
BaBar	$\pi^+\pi^-\mathrm{J}/\psi$	93.4	8.4×10^{-6}	5	4.38
BaBar	$\mathrm{D}\bar{\mathrm{D}}^*$	33.1	1.67×10^{-4}	2.0	1

Table 5. The sets of parameters for the Belle [10, 99] and BABAR [11, 100] data.

Set*	g	E_f, MeV	$f_\rho\times10^3$	$f_\omega\times10^3$	$\mathcal{B}\times10^4$	ϕ, deg	W	$\mathcal{B}W\times10^4$	Re a, fm	$\Gamma(\gamma\psi')$, MeV
$\mathrm{Belle_v}$	0.3	−12.8	7.7	40.7	2.7	180	0.19	0.5	−5.0	$\sim10^3$
$\mathrm{Belle_b}$	0.137	−12.3	0.47	2.71	4.3	153	0.43	1.9	3.5	60
$\mathrm{BaBar_v}$	0.225	−9.7	6.5	36.0	3.9	113	0.24	1.8	−4.9	800
$\mathrm{BaBar_b}$	0.080	−8.4	0.2	1.0	5.7	0	0.58	3.3	2.2	25

* The lower index labels a bound state (b) or a virtual level (v).

The description obtained allows drawing certain conclusions on the nature of X(3872). First, the Belle data unambiguously point to X(3872) being a bound state. Indeed, the description of the data as a virtual level is of a considerably worse quality than under the assumption of a bound state: a virtual level corresponds to a threshold cusp in the inelastic channel, which is incompatible with the $\pi^+\pi^-\mathrm{J}/\psi$ data. For the BABAR data, the description in terms of a virtual level is comparable to the bound-state description. But the estimate of the $\Gamma(\gamma\psi')$ decay width for the virtual level looks unnaturally large in comparison with the values collected in Table 3, while the estimates of the $\Gamma(\gamma\psi')$ width in the case of a bound state are in qualitative agreement with the results in Table 3.

The value W of the integral of the spectral density over the near-threshold region given in Table 5 for the $\mathrm{Belle_v}$ and $\mathrm{BABAR_v}$ sets indicates a rather small admixture of the χ'_{c1} charmonium to the wave function of X, while for the $\mathrm{Belle_b}$ and $\mathrm{BABAR_b}$ sets corresponding to a bound state, this admixture amounts to about 50%.

In the case of the bound state, it is instructive to consider the quantity

$$\mathcal{Z}=\int_{E_{\rm min}}^{E_{\rm max}} w_{\rm inel}(E)\,\mathrm{d}E\,, \tag{113}$$

where

$$w_{\rm inel}(E)=\frac{1}{2\pi\left|D(E)\right|^2}\,\Gamma(E)\,. \tag{114}$$

In the limit of vanishing inelasticity, the spectral density below the $\mathrm{D}^0\bar{\mathrm{D}}^{*0}$ threshold becomes proportional to a

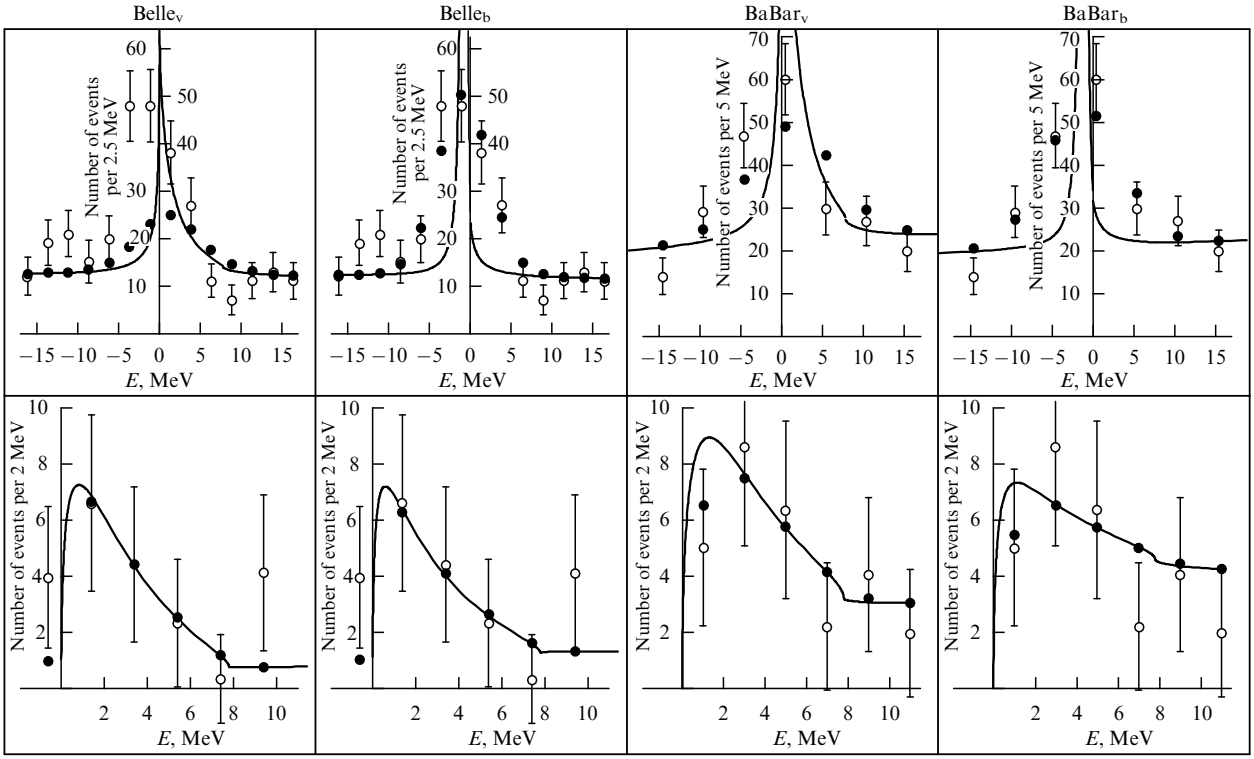

Figure 7. Description of the experimental data on the (a) $\pi^+\pi^-\mathrm{J}/\psi$ and (b) $\mathrm{D}^0\bar{\mathrm{D}}^{*0}$ channels with the parameters given in Table 5. (Adapted from Ref. [93].)

δ-function,

$$w(E<0)\to Z\delta(E-E_{\rm bound})\,, \tag{115}$$

with the coefficient Z being nothing but the Z factor for a true bound state [see definition (40)]. Then the factor $\mathcal{Z}$ can be viewed as the Z factor of X(3872) as a bound state, smeared due to the presence of inelasticity, and it takes the value

$$\mathcal{Z}=0.37 \tag{116}$$

for the Belle data set.

Thus, we conclude that X(3872) is not a *bona fide* charmonium accidentally residing at the $\rm D^0\bar D^{*0}$ threshold. If this were the case, the integral of the spectral density over the resonance region would be unity, but it does not exceed 50% for the found bound-state solutions and is very small for the virtual-state solutions. The X(3872) state is rather generated dynamically by a strong coupling of the bare $\chi'_{\rm c1}$ charmonium to the $\rm D\bar D^*$ hadronic channel, with a large admixture of the $\rm D\bar D^*$ molecular component.

We now comment on the role of the parameter Γ_0. As was discussed above, this parameter accounts for the contribution of the numerous decay modes of the charmonium $\chi'_{\rm c1}$, and it was therefore fixed based on the estimates of the width of this genuine charmonium. We consider the ratio of the elastic branching to the inelastic one [63, 101],

$$\frac{\rm Br(X\to D^0\bar D^0\pi^0)}{\rm Br_{inel}}\,. \tag{117}$$

In the gedanken limit $\Gamma_0=0$, the inelastic modes are exhausted by the $\pi^+\pi^-{\rm J}/\psi$ and $\pi^+\pi^-\pi^0{\rm J}/\psi$ ones. Because the measured branchings for these modes are approximately equal to each other [see Eqn (5)], it suffices to consider the ratio

$$\frac{\rm Br(X\to D^0\bar D^0\pi^0)}{\rm Br(X\to\pi^+\pi^-J/\psi)}\,, \tag{118}$$

which can be estimated with the help of the relation

$$\rm Br(B^+\to K^+X)\,Br(X\to\pi^+\pi^-J/\psi)=(7-10)\times10^{-6}\,, \tag{119}$$

and value (8) for the elastic branching [99]. We find in this way that experimental ratio (118) is large and is approximately 10–15. We reproduce this value for the bound state. The differential rate for the inelastic channels is given by

$$\mathcal{B}\,\frac{1}{2\pi}\,\frac{\Gamma(E)}{\left|D(E)\right|^2}\,, \tag{120}$$

and at $\Gamma_0=0$, the total width $\Gamma(E)$ is defined entirely by the $\rho{\rm J}/\psi$ and $\omega{\rm J}/\psi$ modes and as such is small; thus, it is reasonable to take the limit $\Gamma(E)\to0$. In this limit and in the case of the bound state, distribution (120) becomes proportional to a δ-function and the denominator in ratio (118) becomes a constant. It is then easy to verify that ratio (118) is numerically small (see, e.g., Ref. [26]).

If the condition $\Gamma_0=0$ is relaxed and the inelastic modes are not exhausted by the $\pi^+\pi^-{\rm J}/\psi$ and $\pi^+\pi^-\pi^0{\rm J}/\psi$ ones, ratio (117) is rewritten as

$$\frac{\rm Br(X\to D^0\bar D^0\pi^0)}{\rm Br(X\to\text{not }D^0\bar D^0\pi^0)}\sim1\,, \tag{121}$$

which is quite attainable. Thus, the experimental data are compatible with the assumption of X(3872) being a bound state only if extra nonzero contributions to the total width exist, which come from the decay modes of the charmonium $\chi'_{\rm c1}$. This conclusion is fully in line with the analysis presented above.

On the contrary, for a virtual level, ratio (118) is not restrictive even in the limit $\Gamma_0=0$. Indeed, for the virtual level, the denominator of distribution (120) does not vanish, and hence in the limit $\Gamma(E)\to0$, the denominator in Eqn (118) could be arbitrarily close to zero and therefore ratio (118) could be large (for example, in Ref. [101] this ratio was found to be ≈9.9 for a virtual level). The idea that including an extra inelastic width allows fitting the data on X(3872) with both the virtual and bound state was first put forward in Ref. [102].

To conclude this section, we comment on the width of the $\rm D^*$ meson. In the formulas above, the D^* meson was assumed to be stable while if a finite width of the $\rm D^*$ meson is taken into account, the $\rm D^0\bar D^{*0}\to D^0\bar D^0\pi^0$ decay chain feeds the mass region below the nominal $\rm D^0\bar D^{*0}$ threshold, distorting the $\rm D^0\bar D^{*0}$ line shape in such a way. A refined treatment of such a finite width of a molecule constituent is presented in Ref. [103], while here we estimate these effects using a simple ansatz suggested in Ref. [104] and re-invented in Ref. [63, 105]. The recipe is to make a replacement in the expressions for the $\rm D^0\bar D^{*0}$ momentum entering the formulas for the differential rates,

$$\begin{aligned}&\Theta(E)k_1(E)\to\sqrt{\mu_1}\sqrt{\sqrt{E^2+\Gamma_*^2/4}+E}\,,\\&\Theta(-E)\kappa_1(E)\to\sqrt{\mu_1}\sqrt{\sqrt{E^2+\Gamma_*^2/4}-E}\,,\end{aligned} \tag{122}$$

where Γ_* is the width of the $\rm D^{*0}$ meson. It can be shown [103] that these formulas are valid if the resonance is well separated from the three-body threshold (the $\rm D^0\bar D^{*0}\pi^0$ threshold in this case).

To assess the role of the finite $\rm D^{*0}$ width, we evaluate the $\rm D^0\bar D^{*0}$ differential rates, with $\Gamma_*=63$ keV, for the $\rm Belle_b$ set (the bound-state scenario for the Belle data) and for the $\rm BABAR_v$ set (the virtual-state scenario for the BABAR data) and plot them in Fig. 8 together with the zero-width rates. As can be seen from Fig. 8, accounting for the small finite width of the $\rm D^{*0}$ meson does not change the line shape in the case of the virtual state, while for the bound state, a below-threshold $\rm D^0\bar D^0\pi^0$ peak develops near the bound-state position.

It can be hypothesized that in order to distinguish between the bound- and virtual-state solution, we should seek a below-threshold peak in the $\rm D^0\bar D^0\pi^0$ distribution. Indeed, it is clear from Fig. 8 that the only effect expected is an increase in the number of events in the first near-threshold bin. For the Belle bound-state parameter set $\rm Belle_b$, we have calculated the ratio $\tilde N_i/N_i$ of the number of events in the first ($i=1$) and second ($i=2$) bin, with ($\tilde N_i$) and without (N_i) taking the finite width of the $\rm D^{*0}$ meson into account:

$$\frac{\tilde N_1}{N_1}=4.31\,,\qquad\frac{\tilde N_2}{N_2}=1.01\,. \tag{123}$$

This is illustrated in Fig. 9. The agreement with the experimental data is apparently improved, because the Belle bound-state solutions underestimate the number of events in

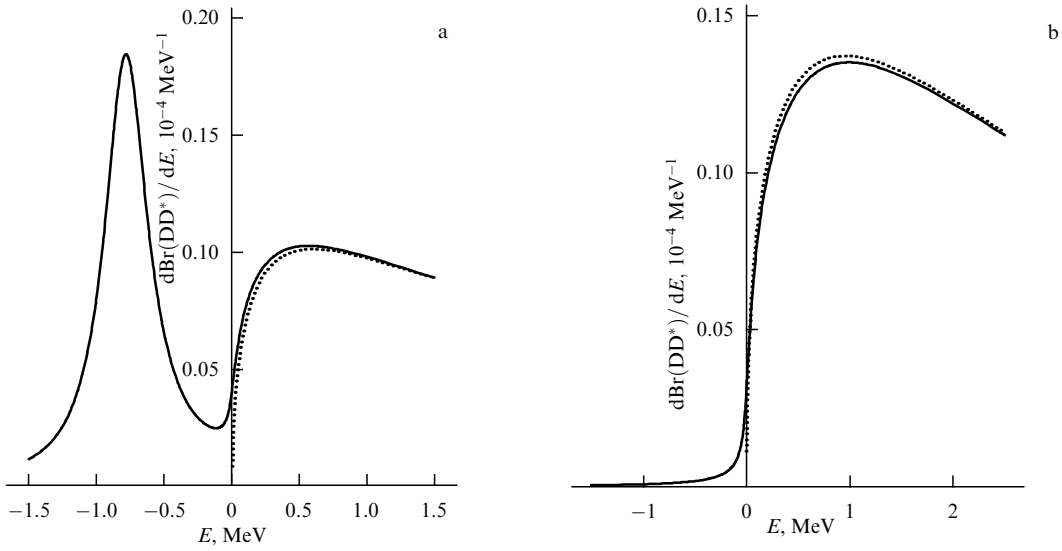

Figure 8. Differential rates for the $D^0\bar{D}^{*0}$ channel given by the formula with a finite width Γ_* included (solid lines) and with a vanishing width (dashed lines) for the (a) Belle_b and (b) BABAR_v parameter sets.

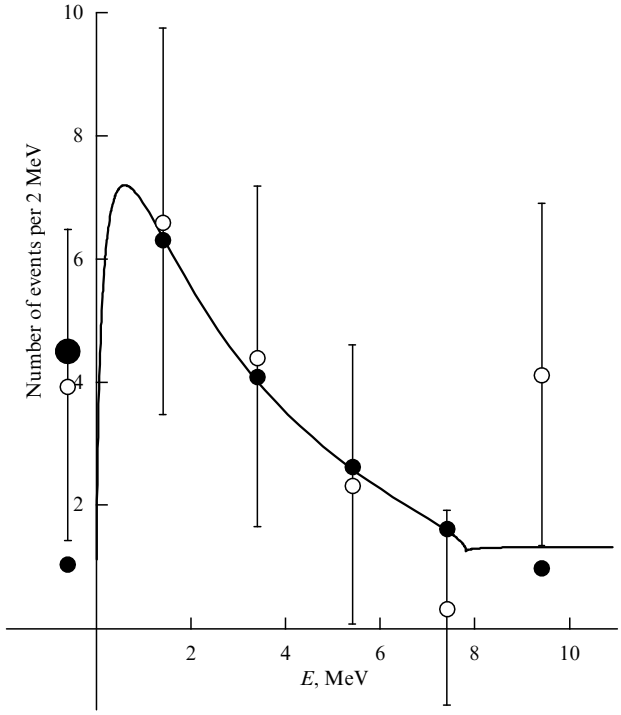

Figure 9. Theoretical description of the Belle data in the $D\bar{D}^*$ channel (Belle_b parameter set). Unfilled circles with error bars correspond to the experimental data, black dots are for the theoretical results; the big dot gives the result of taking the finite width of the D^* meson into account in the formulas. (Adapted from Ref. [93].)

the lowest bin only, and the number of events in higher bins is not affected by the finite-width effects.

Unfortunately, the present experimental situation does not allow identifying the bound-state peak. First, the peak is very narrow, and the existing experimental resolution is too coarse to observe it. Moreover, as was noted in Ref. [63], both the BABAR and Belle collaborations assume that all the $D^0\bar{D}^0\pi^0$ events come from $D^0\bar{D}^{*0}$, distorting the kinematics of the below-threshold events and artificially feeding the above-threshold region at the expense of the below-threshold one.

Related to the question of the finite D^{*0} width is the problem of interference in the decay chains,

$$X(3872) \begin{array}{l} \nearrow \bar{D}^0 D^{0*} \to \bar{D}^0[D^0\pi^0] \searrow \\ \searrow D^0 \bar{D}^{0*} \to D^0[\bar{D}^0\pi^0] \nearrow \end{array} D^0\bar{D}^0\pi^0 . \qquad (124)$$

According to the estimates made in Ref. [106], the interference effects could enhance the below-threshold $D^0\bar{D}^0\pi^0$ rate up to a factor of two; however, the effect is much more moderate above the threshold [103]. A proper account for the interference cannot be done in the over-simplified framework presented in this section but, as was demonstrated above, this effect lies far beyond the accuracy of the existing experimental data.

6. X(3872) and pionic degrees of freedom

From the discussion at the end of Section 5, we conclude that the three-body $D\bar{D}\pi$ threshold is yet another threshold relevant to the X(3872) physics. Indeed, the mass difference between the D^* and D meson is very close to the pion mass, and therefore the two-body $D\bar{D}^*$ cut is close to the three-body $D\bar{D}\pi$ one, and both are close to the X(3872) mass (Fig. 10). Because of this threshold proximity, it is necessary to generalize the coupled-channel scheme used above so as to include the three-body channel explicitly [107].

In reading Section 6.1, it is important to pay attention to the form of the coupled-channel system that incorporates the three-body dynamics [formula (148)] and to the partial wave decomposition of the amplitude described in Eqn (150) and in the text below it. A detailed derivation of these equations can

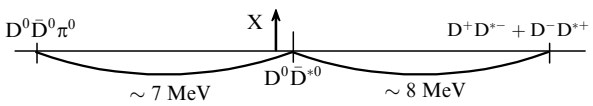

Figure 10. The X(3872) mass relative to the relevant two- and three-body thresholds.

be skipped on the first reading. Section 6.2 and especially its technical part can also be skipped for cursory reading of the review. But it is important to pay attention to the main conclusion made that the one-pion exchange (OPE) is not binding enough to form X(3872) even as a shallow bound state. Another important aspect is the difference between the OPE in the charmonium system under consideration and in the deuteron, the latter being quite often (erroneously) considered a universal standard for such an exchange [see Eqn (155) and the text below it]. Moreover, it follows from the discussions in Section 6.2 that the quantum mechanical problem of the OPE without supplementary short-range interactions is not self-consistent; an appropriate approach based on the effective field theory technique is given in Section 6.3.

6.1 $\mathrm{D\bar{D}^*} \leftrightarrow \mathrm{D\bar{D}\pi} \leftrightarrow \mathrm{\bar{D}D^*}$ coupled-channel system

The basis of the model that incorporates the three-body dynamics in X(3872) comprises three channels

$$|2\rangle = \mathrm{D\bar{D}^*}, \quad |\bar{2}\rangle = \mathrm{\bar{D}D^*}, \quad |3\rangle = \mathrm{D\bar{D}\pi}\,, \tag{125}$$

coupled by pion exchange.

In the center-of-mass frame, the momenta in the two-body $\mathrm{D\bar{D}^*}$ and $\mathrm{\bar{D}D^*}$ systems are defined as

$$\mathbf{p}_{\mathrm{D}} = \mathbf{p}\,, \quad \mathbf{p}_{\bar{\mathrm{D}}^*} = -\mathbf{p}\,, \tag{126}$$

$$\mathbf{p}_{\bar{\mathrm{D}}} = \bar{\mathbf{p}}\,, \quad \mathbf{p}_{\mathrm{D}^*} = -\bar{\mathbf{p}}\,, \tag{127}$$

while in the three-body $\mathrm{D\bar{D}\pi}$ system, it is convenient to define two sets of Jacobi variables $\{\mathbf{p},\mathbf{q}\}$ and $\{\bar{\mathbf{p}},\bar{\mathbf{q}}\}$:

$$\mathbf{p}_{\mathrm{D}} = \mathbf{p}\,, \quad \mathbf{p}_{\bar{\mathrm{D}}} = -\mathbf{q} - \frac{m}{m+m_\pi}\,\mathbf{p}\,, \quad \mathbf{p}_\pi = \mathbf{q} - \frac{m_\pi}{m+m_\pi}\,\mathbf{p} \tag{128}$$

or

$$\mathbf{p}_{\mathrm{D}} = -\bar{\mathbf{q}} - \frac{m}{m+m_\pi}\,\bar{\mathbf{p}}\,, \quad \mathbf{p}_{\bar{\mathrm{D}}} = \bar{\mathbf{p}}\,, \quad \mathbf{p}_\pi = \bar{\mathbf{q}} - \frac{m_\pi}{m+m_\pi}\,\bar{\mathbf{p}}\,, \tag{129}$$

where m is the D-meson mass and m_π is the pion mass. The Jacobi variables from different sets are related as

$$\bar{\mathbf{q}} = \alpha\mathbf{q} + \beta\mathbf{p}\,, \quad \bar{\mathbf{p}} = -\mathbf{q} - \alpha\mathbf{p}\,, \quad \mathbf{q} = \alpha\bar{\mathbf{q}} + \beta\bar{\mathbf{p}}\,, \quad \mathbf{p} = -\bar{\mathbf{q}} - \alpha\bar{\mathbf{p}}\,, \tag{130}$$

where

$$\alpha = \frac{m}{m+m_\pi}\,, \quad \beta = \alpha^2 - 1 = -\frac{(2m+m_\pi)m_\pi}{(m+m_\pi)^2}. \tag{131}$$

The $\mathrm{D^*D\pi}$ vertex is defined as

$$v_{\mathrm{D^*D\pi}}(\mathbf{q}) = g\boldsymbol{\epsilon}\mathbf{q}\,, \tag{132}$$

where $\boldsymbol{\epsilon}$ is the polarization vector of the $\mathrm{D^*}$ meson, $\mathbf{q}$ is the relative momentum in the $\mathrm{D\pi}$ system, and g is the coupling constant, which can be fixed from the experimentally measured $\mathrm{D^*} \to \mathrm{D\pi}$ decay width.

The two-body and three-body channels communicate via the interaction potentials,

$$\begin{aligned} V_{32}^m(\mathbf{p},\mathbf{q};\mathbf{p}') &= gq_m\delta(\mathbf{p}-\mathbf{p}')\,, \\ V_{\bar{3}\bar{2}}^m(\bar{\mathbf{p}},\bar{\mathbf{q}};\bar{\mathbf{p}}') &= g\bar{q}_m\delta(\bar{\mathbf{p}}-\bar{\mathbf{p}}') \end{aligned} \tag{133}$$

and similar potentials V_{23}^m and $V_{\bar{2}\bar{3}}^m$.

The equation for the t-matrix has the form (schematically)

$$t = V - Vg_0t\,, \tag{134}$$

where g_0 is the diagonal matrix of free propagators,

$$\begin{aligned} g_{03}(\mathbf{p},\mathbf{q},M) &= \frac{1}{D_3(\mathbf{p},\mathbf{q},M)}\,, \\ g_{02}(\mathbf{p},M) &= g_{0\bar{2}}(\mathbf{p},M) = \frac{1}{D_2(\mathbf{p},M)}\,. \end{aligned} \tag{135}$$

The inverse two- and three-body propagators are defined as

$$\begin{aligned} D_2(\mathbf{p}) &= m + m_* + \frac{p^2}{2\mu_*} - M\,, \\ D_3(\mathbf{p},\mathbf{q}) &= 2m + m_\pi + \frac{p^2}{2\mu_{\mathrm{p}}} + \frac{q^2}{2\mu_{\mathrm{q}}} - M\,, \end{aligned} \tag{136}$$

where M is the total mass of the system, m_* is the mass of the $\mathrm{D^*}$ meson, the reduced masses are

$$\begin{aligned} \mu_* &= \frac{mm_*}{m+m_*}\,, \quad \mu_{\mathrm{p}} = \frac{m(m+m_\pi)}{2m+m_\pi}\,, \\ \mu_{\mathrm{q}} &\equiv \mu_{\mathrm{q}}(\mathrm{D\pi}) = \frac{mm_\pi}{m+m_\pi}\,, \end{aligned} \tag{137}$$

and we set $\mu_* = \mu_{\mathrm{p}}$ hereafter. Finally, the self-energy part $\Sigma(p)$ due to the virtual $\mathrm{D\pi}$ loop can be written as

$$\Sigma(p) = \frac{g^2}{3}\int\frac{q^2\,\mathrm{d}^3q}{D_3(\mathbf{p},\mathbf{q})}\,. \tag{138}$$

Using definition (138), after some algebraic manipulations, we arrive at the system of equations

$$\begin{cases} t_{22} = -\Sigma + \Sigma D_2^{-1}t_{22} + V_{23}D_3^{-1}V_{32}D_2^{-1}t_{\bar{2}2}\,, \\ t_{\bar{2}2} = -V_{\bar{2}3}D_3^{-1}V_{32} + \Sigma D_2^{-1}t_{\bar{2}2} + V_{\bar{2}3}D_3^{-1}V_{32}D_2^{-1}t_{22} \end{cases} \tag{139}$$

and a similar pair of equations for the $t_{2\bar{2}}$ and $t_{\bar{2}\bar{2}}$ components. A detailed derivation can be found in Ref. [107].

Because the interaction in the system preserves C-parity, it is convenient to define proper combinations of the amplitudes that have a given C-parity,

$$t_\pm = t_{22} \pm t_{\bar{2}2}\,, \tag{140}$$

and satisfy the equations

$$\Delta D_2^{-1}t_\pm = -\Sigma \mp V_{23}D_3^{-1}V_{32} \pm V_{23}D_3^{-1}V_{32}D_2^{-1}t_\pm\,, \tag{141}$$

where

$$\Delta(p) = m_* + m + \frac{p^2}{2\mu_*} - M - \Sigma(p) \tag{142}$$

is the inverse dressed $\mathrm{D^*}$-meson propagator. Then, substituting

$$t_\pm = -\frac{\Sigma D_2}{\Delta} + \frac{D_2}{\Delta}\,a_\pm\,\frac{D_2}{\Delta}\,, \tag{143}$$

we arrive at the expression for the new function $a_\pm^{mn}(\mathbf{p},\mathbf{p}')$:

$$a_\pm = V_\pm - V_\pm\Delta^{-1}a_\pm\,. \tag{144}$$

In what follows, only C-even states are considered, which correspond to the '+' sign above. In addition, we set $V_+ \equiv V$ to simplify the notation.

Now, we define the full form of the one-pion exchange potential V that enters Eqn (144). For this, we explicitly introduce the neutral $(\mathrm{D}^0\bar{\mathrm{D}}^{*0} + \bar{\mathrm{D}}^0\mathrm{D}^{*0})$ and charged $(\mathrm{D}^-\mathrm{D}^{*+} + \mathrm{D}^+\mathrm{D}^{*-})$ two-body channels and take the mass splittings between the charged and neutral particles for both the D mesons and pions into account. This yields

$$V_{ik}^{mn}(\mathbf{p},\mathbf{p}') = (\mathbf{p}' + \alpha_{ik}\mathbf{p})^m (\mathbf{p} + \alpha'_{ik}\mathbf{p}')^n F_{ik}(\mathbf{p},\mathbf{p}'),$$
$$F_{ik}(\mathbf{p},\mathbf{p}') = -\frac{g^2}{D_{3ik}(\mathbf{p},\mathbf{p}')}, \tag{145}$$

where the indices i and k stand for the neutral (0) and charged (c) component, coefficients α are equal to

$$\alpha_{00} = \alpha'_{00} = \frac{m_0}{m_{\pi^0} + m_0}, \quad \alpha_{\mathrm{cc}} = \alpha'_{\mathrm{cc}} = \frac{m_\mathrm{c}}{m_{\pi^0} + m_\mathrm{c}},$$
$$\alpha_{0\mathrm{c}} = \alpha'_{\mathrm{c}0} = \frac{m_\mathrm{c}}{m_{\pi^\mathrm{c}} + m_\mathrm{c}}, \quad \alpha_{\mathrm{c}0} = \alpha'_{0\mathrm{c}} = \frac{m_0}{m_{\pi^\mathrm{c}} + m_0}, \tag{146}$$

and the inverse three-body propagators are

$$D_{300}(\mathbf{p},\mathbf{p}') = 2m_0 + m_{\pi^0} + \frac{p^2}{2m_0} + \frac{p'^2}{2m_0} + \frac{(\mathbf{p}+\mathbf{p}')^2}{2m_{\pi^0}} - M - \mathrm{i}0,$$
$$D_{3\mathrm{cc}}(\mathbf{p},\mathbf{p}') = 2m_\mathrm{c} + m_{\pi^0} + \frac{p^2}{2m_\mathrm{c}} + \frac{p'^2}{2m_\mathrm{c}} + \frac{(\mathbf{p}+\mathbf{p}')^2}{2m_{\pi^0}} - M - \mathrm{i}0,$$
$$D_{30\mathrm{c}}(\mathbf{p},\mathbf{p}') = m_\mathrm{c} + m_0 + m_{\pi^\mathrm{c}} + \frac{p^2}{2m_0} + \frac{p'^2}{2m_\mathrm{c}} + \frac{(\mathbf{p}+\mathbf{p}')^2}{2m_{\pi^\mathrm{c}}} - M - \mathrm{i}0,$$
$$D_{3\mathrm{c}0}(\mathbf{p},\mathbf{p}') = m_\mathrm{c} + m_0 + m_{\pi^\mathrm{c}} + \frac{p^2}{2m_\mathrm{c}} + \frac{p'^2}{2m_0} + \frac{(\mathbf{p}+\mathbf{p}')^2}{2m_{\pi^\mathrm{c}}} - M - \mathrm{i}0. \tag{147}$$

We are interested in the processes with neutral mesons in the final state. The relevant components of the matrix a satisfy the set of equations

$$\begin{cases} a_{00}^{mn}(\mathbf{p},\mathbf{p}') = \lambda_0 V_{00}^{mn}(\mathbf{p},\mathbf{p}') \\ \qquad - \sum\limits_{i=0,\mathrm{c}} \lambda_i \int \dfrac{\mathrm{d}^3 s}{\Delta_i(s)} V_{0i}^{mp}(\mathbf{p},\mathbf{s}) a_{i0}^{pn}(\mathbf{s},\mathbf{p}'), \\ a_{\mathrm{c}0}^{mn}(\mathbf{p},\mathbf{p}') = \lambda_\mathrm{c} V_{\mathrm{c}0}^{mn}(\mathbf{p},\mathbf{p}') \\ \qquad - \sum\limits_{i=0,\mathrm{c}} \lambda_i \int \dfrac{\mathrm{d}^3 s}{\Delta_i(s)} V_{\mathrm{c}i}^{mp}(\mathbf{p},\mathbf{s}) a_{i0}^{pn}(\mathbf{s},\mathbf{p}'), \end{cases} \tag{148}$$

where $\lambda_0 = 1$ and $\lambda_\mathrm{c} = 2$ are the coefficients that take the isospin content of the OPE into account.

The inverse propagators Δ_0 and Δ_c entering system (148) take the form

$$\Delta_0(p) = m_{*0} + m_0 + \frac{p^2}{2\mu_{0*}} - M - \frac{\mathrm{i}}{2}\Gamma_0(p),$$
$$\Delta_\mathrm{c}(p) = m_{*\mathrm{c}} + m_\mathrm{c} + \frac{p^2}{2\mu_{\mathrm{c}*}} - M - \frac{\mathrm{i}}{2}\Gamma_\mathrm{c}(p), \tag{149}$$

where μ_{0*} and $\mu_{\mathrm{c}*}$ are the reduced masses in the respective $\mathrm{D}^0\bar{\mathrm{D}}^{*0} + \bar{\mathrm{D}}^0\mathrm{D}^{*0}$ and $\mathrm{D}^-\mathrm{D}^{*+} + \mathrm{D}^+\mathrm{D}^{*-}$ systems, and the loop operator [see Eqn (142)] is replaced by the running width $\Gamma(p)$ (analytically continued below the threshold), which includes both the self-energy $\Sigma(p)$ and the contributions from the other decay channels of the D^* meson; see Ref. [107].

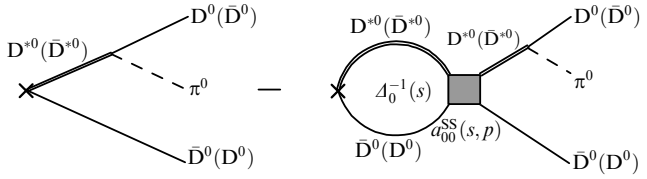

Figure 11. Production amplitude for the $\mathrm{D}^0\bar{\mathrm{D}}^0\pi^0$ final state. The cross stands for a point-like source.

System of equations (148) (together with the system of equations for $a_{0\mathrm{c}}^{mn}$ and a_{cc}^{mn}) is the central result in this section: the equations obtained describe the interaction generated in the $\mathrm{D}\bar{\mathrm{D}}^*$ system by the OPE, which is consistent with the constraints from the three-body unitarity in to the $\mathrm{D}\bar{\mathrm{D}}\pi$ channel.

It is convenient to perform a partial wave decomposition of the amplitude a in terms of the spherical vectors $\mathbf{Y}_{JLM}(\mathbf{n})$,

$$a_{ik}^{mn}(\mathbf{p},\mathbf{p}') = \sum_J \sum_{L_1 L_2} a_{ik}^{J,L_1,L_2}(p,p') \sum_M \bigl(\mathbf{Y}_{JL_1M}(\mathbf{n})\bigr)^m \bigl(\mathbf{Y}^*_{JL_2M}(\mathbf{n}')\bigr)^n, \tag{150}$$

where $\mathbf{n}$ and $\mathbf{n}'$ are the unit vectors for the momenta $\mathbf{p}$ and $\mathbf{p}'$. Because the X(3872) quantum numbers are 1^{++}, two partial waves, S and D, contribute to the amplitude, and we therefore have $J = 1$ and $L_1, L_2 = 0, 2$. If, in addition, we are interested in the S wave in the final state, we need only the a_{ik}^{SS} and a_{ik}^{DS} matrix elements. The explicit form of the potentials entering the equations for these quantities can be found in Ref. [107].

Under the assumption of a point-like source producing a C-even pair $\mathrm{D}^0\bar{\mathrm{D}}^{*0}$ in the S wave, the production amplitude for the final $\mathrm{D}^0\bar{\mathrm{D}}^0\pi^0$ state with an invariant mass M (Fig. 11) is totally determined by the component a_{00}^{SS}; the corresponding explicit expressions can also be found in Ref. [107].

6.2 One-pion exchange in X(3872)

One-boson exchange (ρ, ω, and so on) was suggested long ago [22] as a mechanism that can form a bound state of charmed particles. The possibility for an isosinglet C-even $\mathrm{D}\bar{\mathrm{D}}^*$ system to be bound with OPE was studied in Ref. [25]. Shortly after the discovery of X(3872), the model was revisited in Refs [24, 26], where the $\mathrm{D}\bar{\mathrm{D}}^*$ system was treated in a deuteron-like fashion: the OPE enters the problem in the form of a static potential. Almost immediately, the warning was issued in Ref. [30] that because of the three-body $\mathrm{D}\bar{\mathrm{D}}\pi$ threshold proximity, the pion can go on shell and fail to bind X(3872). As was shown in Ref. [108], the three-body cut effects could play a fatal role in the $\mathrm{D}_\alpha\bar{\mathrm{D}}_\beta$ system if the D_β width is dominated by the S-wave $\mathrm{D}_\beta \to \mathrm{D}_\alpha\pi$ decay. In particular, the bound states in the $\mathrm{D}_\alpha\bar{\mathrm{D}}_\beta$ system predicted in Refs [109, 110] in the static approximation disappear in the continuum if the full three-body treatment is used. In the case of X(3872), the generic decay $\mathrm{D}^* \to \mathrm{D}\pi$ is a P-wave one [see formula (132)], and this extra power of the momentum could in principle attenuate the influence of the cut. The problem, however, deserves a detailed investigation.

With the P-wave vertex involved, the D-meson loop integrals entering the equations derived above diverge and require regularization, which can be performed by introdu-

cing suitable form factors with a cut-off parameter Λ. Then the conclusion as to whether the OPE is able to bind X(3872) can be made based on the values of the cutoff Λ needed to produce a shallow bound state. Namely, the existence of a bound state for a relatively small value $\Lambda \lesssim 1$ GeV can be interpreted as proof that the OPE provides enough attraction to produce a bound state, because such values of Λ can be justified in the quark model. On the other hand, larger values of Λ should be disregarded as unphysical. The corresponding calculations were performed in the static limit, and the results were presented in Refs [111, 112]. It is important to note that a bound state in the $D^0\bar{D}^{*0}$ system was found in [111] for the values of Λ about 6–8 GeV. In [112], the charged channel was also taken into account, which allowed the authors to find a bound state for a much smaller cutoff, $\Lambda \simeq 0.6-0.8$ GeV. Thus, the conclusion in Ref. [112] was that X(3872) could be bound by OPE. In [113], the OPE in the X(3872) system was considered beyond the static limit, and it was shown that no bound state existed in the X(3872) system for reasonable values of Λ. In view of the importance of this result for our presentation in what follows, we discuss it here.

To have better contact with previous work, we define a covariant $D^* \to D\pi$ vertex

$$v_\mu = g_f\, \bar{u}^*_\alpha (\tau^a)^\alpha_\beta u^\beta \pi^a p_{\pi\mu}\,, \tag{151}$$

where $p_{\pi\mu}$ is the pion 4-momentum and u^*, u, and π are the isospin wave functions of D^*, D, and the pion. In [112], an effective coupling parameter V_0 was introduced as

$$\frac{g_f^2}{4m_*^2} = \frac{6\pi V_0}{m_\pi^3}\,, \tag{152}$$

with $V_0 \approx 1.3$ MeV extracted from the experimental value [4] of the width

$$\Gamma(D^{*+} \to D^0\pi^+) = \frac{g_f^2 q_{0c}^3}{12\pi m_{*c}^2} = 2V_0\,\frac{q_{0c}^3}{m_\pi^3}\,, \tag{153}$$

where q_{0c} is the relative momentum in the $D^0\pi^+$ system.

We redefine the $D^*D\pi$ vertex (132) and introduce a form factor that controls its behavior at large momenta,

$$\mathbf{g}(\mathbf{q}) = g\mathbf{q}\,\frac{\Lambda^2}{\Lambda^2 + \mathbf{q}^2}\,, \qquad g = \frac{\sqrt{6\pi V_0}}{m_\pi^{3/2}}\,, \tag{154}$$

where the cutoff Λ is introduced as discussed above. If we ignore the isospin symmetry breaking, the OPE potential in the static limit expressed in terms of this vertex takes the form

$$V^{mn}_{\rm stat}(\mathbf{q}) = -\frac{3}{(2\pi)^3}\,\frac{g_m(\mathbf{q})g_n(\mathbf{q})}{\mathbf{q}^2 + \left[m_\pi^2 - (m-m_*)^2\right]}\,, \tag{155}$$

where the factor 3 corresponds to the isosinglet state. We note here that potential (155) is half the one used in Ref. [112]. This means that the coupling V_0 used in Ref. [112] is effectively two times larger than the value $V_0 = 1.3$ MeV found from data on the D^* pionic decays.

It is relevant to comment on a critical difference between the OPE potential in nucleon physics (for example, in the deuteron) and in the physics of the charmonium. If the masses of the particles exchanging the pion are close to one another ($m_* \approx m$) and their mass difference can be disregarded compared with the pion mass (this condition is obviously satisfied for the proton and neutron mass), then potential (155) reduces to a Yukawa one, the standard pion exchange potential in the physics of nucleons. To some extent, this condition is also true in the b-quark sector because the mass difference for the B^* and B mesons equals 45 MeV, one third of the pion mass. However, the situation is totally different in the physics of the charmonium because the mass difference between the D^* and D mesons nearly (within 7 MeV) coincides with the pion mass. Besides that, $m_* - m > m_\pi$, and therefore the parameter $\mu = [m_\pi^2 - (m-m_*)^2]^{1/2}$, which enters the denominator of potential (155) and determines its behavior, is not only small in absolute value but also is purely imaginary, and hence instead of an exponential falloff with the distance between the mesons, the static potential oscillates. It is also important to note that the numerical smallness of the parameter μ emphasizes the low accuracy of the static approximation for X(3872) in general, because disregarding the D-meson recoil terms in the denominator of the potential does not look like a well-justified procedure. In a more accurate approach, such terms are retained [see, e.g., expressions for the inverse three-body propagators (147) with the three-body dynamics included]. Below, this problem and its implications for the OPE potential are discussed in more detail.

Potential (155) can be written as

$$V^{mn}_{\rm stat}(\mathbf{q}) = -\frac{3}{(2\pi)^3}\,g_m(\mathbf{q})g_n(\mathbf{q})\left(V_1^{\rm stat}(\mathbf{q}) + V_2^{\rm stat}(\mathbf{q})\right),$$

$$V_1^{\rm stat}(\mathbf{q}) = \frac{1}{2E_\pi(E_\pi + m - m_*)}\,, \tag{156}$$

$$V_2^{\rm stat}(\mathbf{q}) = \frac{1}{2E_\pi(E_\pi + m_* - m)}\,, \tag{157}$$

where $E_\pi = \sqrt{\mathbf{q}^2 + m_\pi^2}$. This corresponds to two different orderings (contributions of the intermediate $D\bar{D}\pi$ and $D^*\bar{D}^*\pi$ states) in the framework of the time-ordered perturbation theory (see the graphs in Fig. 12).

Because $m_* \approx m + m_\pi$, we have $V_1 \gg V_2$ for the momenta q of the order of several hundred MeV. However, as demonstrated above, the static approximation is not valid for such momenta. On the other hand, for higher momenta, we should take the contribution of the second ordering into account. This opens a Pandora's box of intermediate states available via the transition chain

$$\bar{D}^*D^*\pi \leftrightarrow \bar{D}D^*\pi\pi \leftrightarrow \bar{D}D\pi\pi\pi\ldots, \tag{158}$$

invalidating, inter alia, the very notion of a single-pion exchange.

We now consider the OPE potential beyond the static limit. We first note that for a given formulation of the

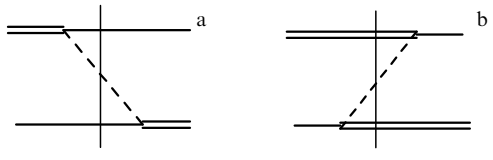

Figure 12. Diagrams in the Time-Ordered Perturbation Theory corresponding to the potentials V_1 (a) and V_2 (b). The double and single solid lines are for the D^* and D mesons, respectively, while the dashed line is for the pion. The thin vertical line pinpoints the intermediate state.

problem, all momenta $q \lesssim \Lambda$ are allowed. Therefore, once the expected values of the cutoff are large, $\Lambda \lesssim 1$ GeV, we have to resort to relativistic kinematics and modify the potential accordingly, that is, write it as

$$V_{ik}^{mn}(\mathbf{p},\mathbf{p}') = -\frac{1}{(2\pi)^3}\frac{g_m(\mathbf{p}'+\alpha_{ik}\mathbf{p})g_n(\mathbf{p}+\alpha_{ik}\mathbf{p}')}{D_{3ik}(\mathbf{p},\mathbf{p}')}\,, \quad (159)$$

where the vertex $\mathbf{g}(\mathbf{q})$ is given in Eqn (154) and the relativisticized three-body propagator is

$$D_3(\mathbf{p},\mathbf{p}') = 2E_\pi(E_\pi - \mu - \mathrm{i}0)\,, \quad (160)$$

where

$$\mu = m_{*0} + m_0 + E - \sqrt{m^2+p^2} - \sqrt{m'^2+p'^2}\,, \quad (161)$$

$$E_\pi = \sqrt{(\mathbf{p}+\mathbf{p}')^2 + m_\pi^2}\,. \quad (162)$$

Here, as before, the energy E is defined relative to the neutral two-body $\mathrm{D}^0\bar{\mathrm{D}}^{*0}$ threshold and the coefficients α and α' can be found from the standard relativistic textbook formula (see, e.g., textbook [114] or paper [115]),

$$\begin{aligned}\alpha &= \frac{1}{\sqrt{\varepsilon'^2-p^2}}\left[\sqrt{m'^2+p'^2} + \frac{\mathbf{p}\mathbf{p}'}{\varepsilon'+\sqrt{\varepsilon'^2-p^2}}\right],\\ \alpha' &= \frac{1}{\sqrt{\varepsilon^2-p'^2}}\left[\sqrt{m^2+p^2} + \frac{\mathbf{p}\mathbf{p}'}{\varepsilon+\sqrt{\varepsilon^2-p'^2}}\right],\end{aligned} \quad (163)$$

where

$$\varepsilon = \sqrt{m^2+p^2} + E_\pi\,, \qquad \varepsilon' = \sqrt{m'^2+p'^2} + E_\pi.$$

The kinematics corresponding to this potential are detailed in Fig. 13. It is clear that potential (159) is nothing but the V_1 part of the OPE beyond the static limit. The static approximation is obtained from expression (159) by setting $\alpha = \alpha' = 1$ and $\mu = m_{*0} + m_0 - m - m'$. Neither replacement is insignificant, especially the former one: α decreases with the increase in the momentum, which leads to an effective suppression of the potential compared to the naive static approximation with $\alpha = \alpha' = 1$.

Moreover, the two-body propagators $\Delta_0(p)$ and $\Delta_c(p)$ in Eqn (148), as well as the three-body propagator $D_{3ik}(\mathbf{p},\mathbf{p}')$, generate contributions to the imaginary part of the interaction, which must be kept in order to preserve unitarity but which are obviously omitted in Refs [111, 112]. These contributions also effectively weaken the interaction.

The strategy employed in Ref. [113] to resolve the problem of the OPE as a binding force is as follows. System of

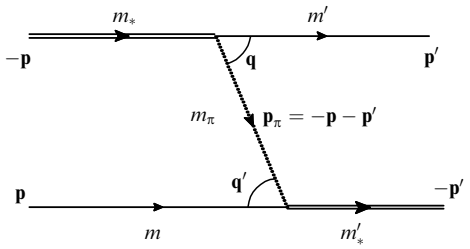

Figure 13. Kinematics of D^* meson scattering on a D meson due to OPE.

Table 6. Minimal cut-off parameter $\Lambda_{\min}$ consistent with a bound state in the $\mathrm{D}\bar{\mathrm{D}}^*$ system.

	V_1^{stat}	$V_1^{\mathrm{stat}} + V_2^{\mathrm{stat}}$	V_1	$V_1 + V_2^{\mathrm{stat}}$
$\Lambda_{\min}$, MeV	2750	1650	3800	2100

equations (148) is solved for various versions for the potential, and the X(3872) differential production rate is then calculated. A bound-state singularity, if it exists, reveals itself as a below-threshold peak in the production rate. For a fixed value of the coupling ($V_0 = 1.3$ MeV), once the potential becomes more attractive with the cut-off growth, there is a minimal value of the cutoff Λ for which a bound state appears right at the two-body threshold. The results for such boundary cut-offs are listed in Table 6, from which we can see that, on the one hand, even the inclusion of the second ordering and the use of the static limit do not lead to phenomenologically acceptable values of Λ and, on the other hand, effects related to dynamical pions increase the minimal Λ.

We are therefore forced to conclude that OPE is not strong enough to bind X(3872), and some other short-range dynamics are responsible for its binding.

6.3 Elastic line shape of X(3872) with the three-body dynamics included

Results obtained in Section 6.5 allow concluding that a more appropriate approach to the description of X(3872) is a field-theory approach in which the OPE interaction is well defined only in combination with a contact term that describes the short-range part of the interaction (including the short-range part of OPE) [107, 116]. Large momenta (of the order of the cutoff) do not enter into such a formulation because they are absorbed into a renormalized contact term and the dynamics of the system occur at momenta of the order of the binding momentum scale $k_{\mathrm{b}} \simeq \sqrt{mE_{\mathrm{b}}}$, that is, momenta of the order of several tens of MeV. In this case, it is quite legitimate to use nonrelativistic kinematics for all particles (including pions).

Following this idea, we parameterize the short-range part of the potential by a constant $C_0(\Lambda)$, where Λ is a regulator (for simplicity, a sharp cutoff in the three-dimensional momentum by the step-like function $\theta(\Lambda - |\mathbf{p}|)$ is used in the integrals). For a given value of Λ, this contact term is fixed by the value of the X(3872) binding energy, which we set equal to 0.5 MeV for definiteness. In such a way, $C_0(\Lambda)$ absorbs the leading dependence of the observables on the cutoff, while the residual dependence is expected to be rather weak. Otherwise, we would have to introduce additional, momentum-dependent counter terms.

Before we proceed to solving the full problem, we consider a simple analytically solvable model in which the potential is exhausted by contact interaction. We then have the following system of equations for the amplitudes $a_{00} \equiv a_{00}^{SS}$ and $a_{c0} \equiv a_{\mathrm{c}0}^{SS}$:

$$\begin{cases} a_{00} = C_0 - C_0 a_{00} I_0 - 2C_0 a_{\mathrm{c}0} I_{\mathrm{c}}\,,\\ a_{\mathrm{c}0} = 2C_0 - 2C_0 a_{00} I_0 - C_0 a_{\mathrm{c}0} I_{\mathrm{c}}\,, \end{cases} \quad (164)$$

with the solution for a_{00} given by

$$a_{00} = \frac{C_0(1-3C_0 I_{\mathrm{c}})}{(1+C_0 I_0)(1+C_0 I_{\mathrm{c}}) - 4C_0^2 I_0 I_{\mathrm{c}}}\,. \quad (165)$$

For the loop integrals, we can use the expansion

$$I_0 = \int_0^\Lambda \mathrm{d}q\, \frac{q^2}{q^2/(2\mu_{0*}) - E - \mathrm{i}0} \approx 2\mu_{0*}\left(\Lambda + \frac{\mathrm{i}}{2}\,\pi k_0 - \frac{k_0^2}{\Lambda}\right) + O\left(\frac{k_0^4}{\Lambda^3}\right), \tag{166}$$

$$I_\mathrm{c} = \int_0^\Lambda \mathrm{d}q\, \frac{q^2}{q^2/(2\mu_{\mathrm{c}*}) + \Delta - E - \mathrm{i}0} \approx 2\mu_{\mathrm{c}*}\left(\Lambda + \frac{\mathrm{i}}{2}\,\pi k_\mathrm{c} - \frac{k_\mathrm{c}^2}{\Lambda}\right) + O\left(\frac{k_\mathrm{c}^4}{\Lambda^3}\right), \tag{167}$$

where $k_0^2 = 2\mu_{0*}E$, $k_\mathrm{c}^2 = 2\mu_{\mathrm{c}*}(E-\Delta)$, and $\Delta = (m_{*\mathrm{c}} + m_\mathrm{c}) - (m_{*0} + m_0) \approx 8$ MeV. The requirement that the pole of scattering amplitude (165) exist at $E = -E_\mathrm{b}$ leads to the quadratic equation

$$\big(1 + C_0 I_0(-E_\mathrm{b})\big)\big(1 + C_0 I_\mathrm{c}(-E_\mathrm{b})\big) - 4C_0^2 I_0(-E_\mathrm{b}) I_\mathrm{c}(-E_\mathrm{b}) = 0 \tag{168}$$

for the counter term C_0, with two solutions. These solutions correspond to different values of the isospin, and we have to select one for the isoscalar X(3872) state.

We now consider the full problem, which includes, together with the contact interaction, the OPE potential derived in Section 6.1. As discussed above, the value of the contact term C_0 is chosen so as to ensure the existence of a bound state with a given energy. The dependence $C_0(\Lambda)$ shown in Fig. 14 is rather nontrivial. This type of behavior (the so-called limit cycle) is typical of such kinds of calculations (see, e.g., Refs [117–121], where a similar behavior was observed in nucleon systems). Indeed, with the increase in the cutoff Λ, the long-range part of the interaction varies, and therefore a new value of the contact term is needed to compensate for this variation and keep the bound state in place. Near the discontinuity point of the $C_0(\Lambda)$ curve, small variations in the cutoff lead to large variations in C_0. At some critical value of the cutoff, it becomes impossible to adjust C_0, and hence the level under consideration sinks and the next level is fixed at the given binding energy, thus performing a hop to the next branch of the function $C_0(\Lambda)$. This cycle then repeats itself. As was explained above, the two solutions for C_0 at each Λ correspond to the two values of the isospin of the system. For X(3872), we should consider $I = 0$, which is described by the red curve in Fig. 14. We note that the C_0 vanishing at some value of the cutoff cannot be interpreted as the absence of short-range dynamics in the system, because the choice of the cutoff and the corresponding redefinition of the short-range and long-range contributions to the dynamics do not affect observable quantities, which is guaranteed by the renormalization group equations (by the requirement that $\partial E_\mathrm{b}/\partial\Lambda = 0$ in this case). The residual Λ-dependence can be removed by additional contact terms of a higher order, which is not required in this particular case because such a residual Λ-dependence is very weak, about a few percent (see the discussion below) and can be treated as a theoretical uncertainty of the calculation.

To increase the accuracy, it is convenient to fix the value of the cutoff in the plateau region, where a reasonable choice is $300 \lesssim \Lambda \lesssim 1700$ MeV or $2500 \lesssim \Lambda \lesssim 3800$ MeV. As was discussed in Section 6.2, using large cutoffs requires relativistic dynamics, and it therefore makes sense to consider not very large cutoffs in order to have momenta in the renormalized theory small compared with the particle masses, that is, for the nonrelativistic approximation to be applicable. Thus, it proves convenient to fix the value $\Lambda = 500$ MeV, which falls into the first interval above.

The results for the calculated line shape of X(3872) in the $\mathrm{D}^0\bar{\mathrm{D}}^0\pi^0$ channel are shown in Fig. 15. The following three cases were investigated:

(1) Single-channel problem (only the neutral channel $\mathrm{D}^0\bar{\mathrm{D}}^{*0}$) in the static approximation with the imaginary part of the potential ignored and with a constant value used in the two-body propagator Δ_0 instead of the running width.

(2) Single-channel approximation for the full dynamical problem, including intermediate three-body $\mathrm{D}\bar{\mathrm{D}}\pi$ states and the dynamical width of the D^* meson with the omitted contribution of charged pions.

(3) Full dynamical two-channel problem with the three-body $\mathrm{D}\bar{\mathrm{D}}\pi$ dynamics and the dynamical ('running') width of D^* taken into account.

All three curves in Fig. 15 are normalized near the three-body threshold $\mathrm{D}^0\bar{\mathrm{D}}^0\pi^0$ at $E = -7.15$ MeV. It is clearly seen that the difference between cases 2 and 3 is not large, which is readily explained by the position of charged three-body thresholds $\mathrm{D}^+\bar{\mathrm{D}}^0\pi^-$, $\mathrm{D}^-\mathrm{D}^0\pi^+$, and $\mathrm{D}^+\mathrm{D}^-\pi^0$, which are

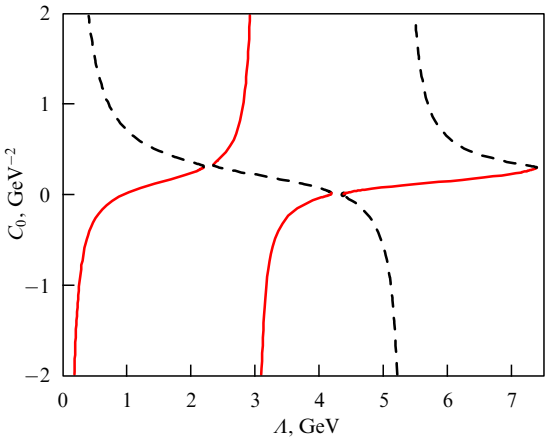

Figure 14. Behavior of the contact term C_0 as a function of the cutoff Λ in the full problem with pions. (Adapted from Ref. [107].)

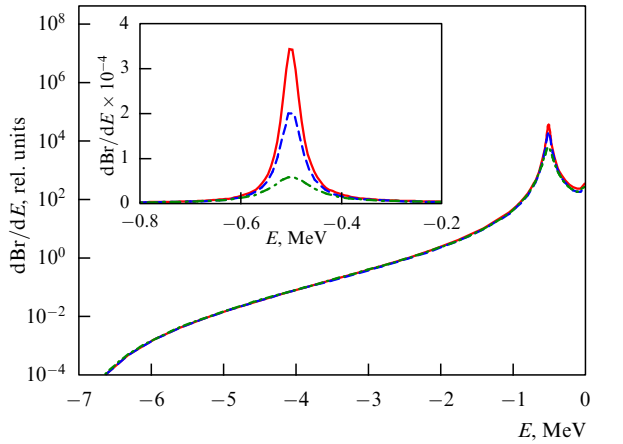

Figure 15. X(3872) production rate (on a log scale) in the $\mathrm{D}^0\bar{\mathrm{D}}^0\pi^0$ channel for three cases: (1) single-channel calculation in the static approximation (green dashed-dotted line); (2) single-channel dynamical calculation (blue dashed line); (3) full two-channel dynamical calculation (red solid line). The enlarged peak region is shown in the inset on a linear scale. (Adapted from Ref. [107].)

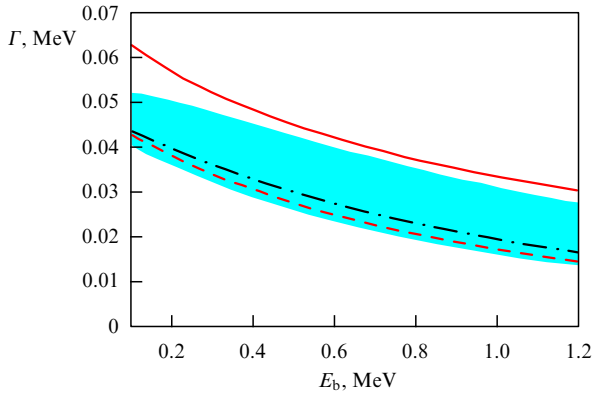

Figure 16. Width of X(3872) as a function of the binding energy E_b. The red dashed line shows the result of the full dynamical calculation, the respective black dashed line and the blue band show X-EFT results in the leading [106] and next-to-leading [122] orders. The solid red line shows the full width, including the contribution of the decay $D^* \to D\gamma$. (Adapted from Ref. [107].)

located sufficiently far from the peak. On the other hand, the difference between cases 1 and 2 is substantial, and elucidates the role of the three-body dynamics in X(3872): inclusion of the three-body effects makes the resonance narrower by a factor of 2 (see details of the calculation in Ref. [107]).

We note that the dependence of the results on the value of the cutoff is weak. The results shown were obtained for the cutoff $\Lambda = 500$ MeV; however, variations in the cutoff in a rather wide interval (test calculations were performed for $300 \lesssim \Lambda \lesssim 1700$ MeV) result in variations in the line shape at the level of several percent [107].

It is instructive to compare the results of the full two-body dynamical calculations with similar results obtained in the framework of a perturbative description of pions, the so-called effective field theory for X(3872) (X-EFT). The width in the leading order was calculated in Ref. [106], and this result was improved in Ref. [122] by considering next-to-leading-order corrections, which is a natural generalization of the approach developed for nucleon–nucleon systems in Ref. [123]. The results of the comparison shown in Fig. 16 confirm the possibility of considering the pionic contribution in the framework of the perturbation theory, at least for the problem of the shape of the below-threshold peak in the X(3872) system. We note, however, that the suggested approach has a much wider domain of applicability. In particular, it allows a natural generalization to other near-threshold states, including those for which the threshold mass difference is not as small as for X(3872). In this case, the possibility of treating pions perturbatively is questionable. Examples of such states are the $D^{(*)}\bar{D}^{(*)}$ and $B^{(*)}\bar{B}^{(*)}$ systems, and a universal approach to these states based on the heavy-quark spin symmetry was suggested in Ref. [124] and further developed in [83, 87, 125]. Examples of the application of this nonperturbative approach to the aforementioned systems can be found in Refs [85, 88].

7. Remark on lattice calculations for X(3872)

QCD lattice calculations performed from first principles are known to be an alternative source of information on hadronic states, in addition to real experiments. Due to the fast growth of computer power and the appearance of a large number of high-productivity computer clusters, modern lattice calculations are able to answer many questions related to the physics of strong interactions.

Recently, the first results of lattice calculations for exotic states in the charmonium spectrum have started to arrive, in particular, for X(3872) [126–128]. Unfortunately, at the moment, all such calculations suffer from certain shortcomings. First, their accuracy is quite low. For example, the X(3872) binding energy found in Ref. [126] is

$$E_b = 11 \pm 7 \text{ MeV}, \tag{169}$$

with the uncertainty being of the order of the central value. The results reported in Refs [127, 128] are quite similar. In addition, the size of the lattice used, $L \simeq 2$ fm, is definitely not large enough to reliably describe near-threshold states with a wave function containing a long-range molecular component [129]. Finally, all such calculations are performed for a relatively large current mass of the u and d quarks (it proves convenient to deal with the pion mass instead of the quark mass because they are uniquely interrelated through the Gell-Mann–Oakes–Renner relation [130]).

Most of the above shortcomings can be amended only by improving the numerical methods and increasing computer power. However, the problem of the unphysical pion mass used on the lattice can be reduced to a large extent with the help of the approach used in Refs [131, 132] and described below. Indeed, in all calculations performed above, the pion mass enters as a parameter whose value can be varied freely (preserving a hierarchy of scales, which plays an important role for the formulation of the coupled-channel problem) and, notably, can be increased to the value $m_\pi = 266$ MeV used in lattice calculations [126–128]. An important prerequisite for such an adiabatic variation of the pion mass in the equations is a full (preferably nonperturbative) account of three-body dynamics in the equations, which is substantially affected by the pion mass change. Coupled-channel equations (148) derived above meet this condition, allowing us to use them in solving the problem of the chiral extrapolation of the X(3872) binding energy from the physical pion mass to an unphysically large mass used on the lattice [131, 132].

The main problem encountered in building the chiral extrapolation for the X(3872) binding energy is the unknown nature of the short-range forces responsible for its formation. As a result, the dependence of the contact term C_0 on m_π can only be established by resorting to the idea of its natural behavior. If applied to the problem at hand, naturalness implies the absence of anomalously large or small mass scales and coefficients. This appears to be sufficient to explain the results obtained on the lattice: Fig. 17 demonstrates that, on the one hand, the increase in the binding energy with the pion mass growth predicted by the lattice can be explained naturally in the molecular model for X(3872) and, on the other hand, the role of pionic dynamics in this calculation is quite important: it suffices to compare the predictions of the pionless theory (the dashed-dotted line in Fig. 17) with the predictions of the full theory (the black and red bands). A detailed description of the chiral extrapolations for X(3872) can be found in Refs [131, 132].

Further discussion of lattice calculations for X(3872) goes beyond the scope of this review, devoted to various phenomenological aspects of the description and interpretation of this

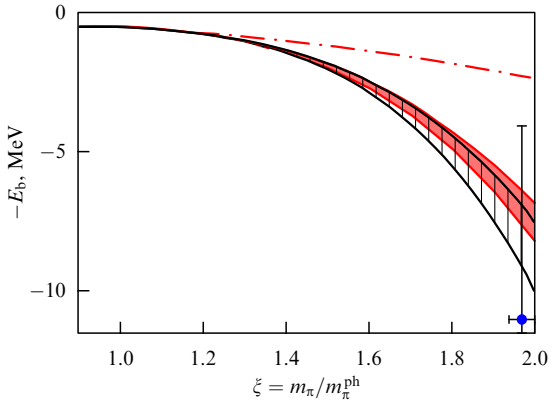

Figure 17. Dependence of the X(3872) binding energy on the pion mass. The black and red bands correspond to the calculations performed in the framework of nonrelativistic [131] and relativistic approaches [132]. The dashed-dotted line shows the result obtained in a purely contact theory without pions. The blue dot with error bar gives the lattice result reported in Ref. [128]. Adapted from Ref. [132].

exotic state. We note, however, that regardless of the perspectives of the studies of exotic states on the lattice, building chiral extrapolations can be viewed as an important theoretical problem for near-threshold resonances in and of itself because it allows investigating the contribution and interplay of different dynamics defined and acting at different energy scales.

8. Radiative decays of X(3872)

Radiative decay modes of X(3872) into $\gamma J/\psi$ and $\gamma\psi'$ final states are among the experimentally studied processes; in particular, the ratio of the branching fractions of these processes has been measured [see Eqn (16)]. Because radiative transitions offer a rather powerful tool to study the meson wave function and to choose the most appropriate model, a theoretical study of these decays is quite a natural next step.

Qualitatively, such radiative modes were taken into account in the data analysis discussed in Section 5. Namely, the requirement was imposed on the fit for the $X \to \gamma\psi'$ decay width to be in accord with the model estimates for the χ'_{c1} charmonium. If we assume that the X(3872) radiative decays proceed solely via the quark component of its wave function, experimental ratio (16) is easily reproduced. Phenomenological estimates presented in some papers (see, e.g., [133–135]) demonstrate that even a small admixture (around 5–12%) of the $\bar{c}c$ quarkonium in the X(3872) wave function suffices to explain the experimental data. On the other hand, there is an opinion expressed in the literature that it is impossible to obtain this kind of ratio (and, more generally, a ratio R comparable to unity) in the molecular picture (see, e.g., Ref. [136]).

In this section, we show that under quite natural assumptions on the model parameters (in particular, on the ratio of the coupling constants of the charmonia J/ψ and ψ' with D mesons), experimental ratio (16) can also be reproduced in the molecular picture. Here, we follow Ref. [137]. On the first reading of this review, this section can be skipped, especially the technical details of the derivation of the radiative decay amplitude for X(3872). But it is important to pay attention to the conclusions at the end of the section, which state that the data on radiative decays cannot be decisive in verifying the molecular nature of X(3872) because they are much more sensitive to the short-range part of its wave function.

The amplitude of the radiative decay $X \to \gamma\psi$ (where $\psi = J/\psi$ or ψ') is given by a sum of the graphs depicted in Fig. 18. The radiative transition could proceed either via the $\bar{c}c$ component of the X(3872) wave function (Fig. 18f) or via its mesonic component (Figs 18a–e), and the latter mechanism dominates if X(3872) is a mesonic molecule.

We temporarily assume that X(3872) is a pure $D\bar{D}^*$ molecule and present the vertex $X_\sigma(p) \to D\bar{D}^*_\tau(k)$ (where σ and τ are the respective polarization vector indices of X(3872) and D^*) in the form

$$\Gamma^{(X)}_{\sigma\tau}(p,k) = \frac{1}{\sqrt{2}}\, x_{\rm nr}\sqrt{M_X m_* m}\, g_{\sigma\tau}\,, \tag{170}$$

where m, m_*, and M_X are the respective masses of D, D^*, and X(3872) and $x_{\rm nr}$ is the nonrelativistic coupling constant, which can be extracted from the X(3872) binding energy [60, 138].

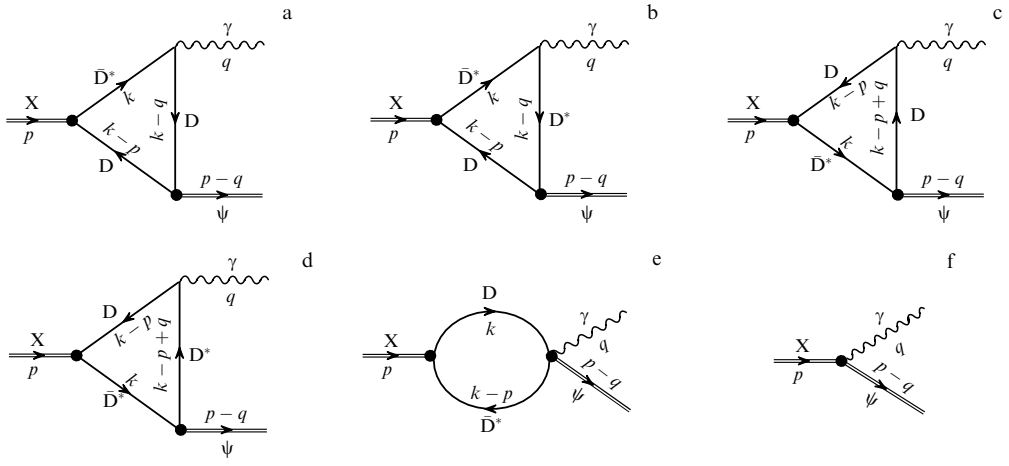

Figure 18. (a)–(e) Graphs describing the radiative transition $X(3872) \to \gamma\psi$, where $\psi = J/\psi$ or ψ' in the mesonic loop mechanism. The charge-conjugate loops are not shown but are included in the calculation. (f) Graph for the contribution of the compact component of the X wave function.

The $\psi_\nu(p) \to \bar{\mathrm{D}}(k_1)\mathrm{D}(-k_2)$, $\psi_\nu(p) \to \bar{\mathrm{D}}^*_\tau(k_1)\mathrm{D}(-k_2)$, and $\psi_\nu(p) \to \bar{\mathrm{D}}^*_\alpha(k_1)\mathrm{D}^*_\beta(-k_2)$ transition vertices can be written as

$$V^{\bar{\mathrm{D}}\mathrm{D}}_{\nu}(k_1,-k_2) = g_2\sqrt{m_\psi}m(k_1+k_2)_\nu\,, \tag{171}$$

$$V^{\bar{\mathrm{D}}\mathrm{D}^*}_{\nu\tau}(k_1,-k_2) = 2g_2\sqrt{\frac{m_\psi m}{m_*}}\epsilon_{\nu\tau\alpha\beta}k_2^\alpha k_1^\beta\,, \tag{172}$$

$$V^{\bar{\mathrm{D}}^*\mathrm{D}^*}_{\nu\alpha\beta}(k_1,-k_2) = g_2\sqrt{m_\psi}m_*\big[(k_1+k_2)_\nu g_{\alpha\beta} - (k_1+k_2)_\beta g_{\nu\alpha} - (k_1+k_2)_\alpha g_{\mu\beta}\big]\,, \tag{173}$$

where heavy-quark symmetry relations are used [139–141].

Electric couplings of a photon to the D mesons are obtained from gauging the corresponding terms of the interaction Lagrangian. Namely, the electric vertex $\mathrm{D}^\pm(k_1) \to \mathrm{D}^\pm(k_2)\gamma_\rho(q)$ $(k_1 = k_2 + q)$ is given by

$$\Gamma^{(\mathrm{e})}_\rho(k_1,k_2) = e(k_1+k_2)_\rho\,, \qquad q = k_1 - k_2\,, \tag{174}$$

where e is the electric charge. Similarly, the electric vertex $\mathrm{D}^{*\pm}_\nu(k_1) \to \mathrm{D}^{*\pm}_\tau(k_2)\gamma_\rho(q)$ $(k_1 = k_2 + q)$ is

$$\Gamma^{(\mathrm{e})}_{\nu\tau\rho}(k_1,k_2) = e\big[(k_1+k_2)_\rho g_{\nu\tau} - k_{1\tau}g_{\nu\rho} - k_{2\nu}g_{\tau\rho}\big]\,. \tag{175}$$

It can be easily verified that both the above vertices satisfy the appropriate Ward identities. Finally, gauging vertex (172) yields a four-point vertex $\mathrm{D}\bar{\mathrm{D}}^*\psi\gamma$ (see the graph in Fig. 18e).

Magnetic transition vertices $\mathrm{D}^{*a}_\nu(k_1) \to \mathrm{D}^{*b}_\tau(k_2)\gamma_\rho(q)$ and $\mathrm{D}^{*a}_\nu(k_1) \to \mathrm{D}^b(k_2)\gamma_\rho(q)$ $(k_1 = k_2 + q)$ follow from the covariant generalization of the chiral Lagrangian in Refs [142, 143] in the form

$$\Gamma^{(m)ab}_{\nu\tau\rho}(q) = em_*(q_\tau g_{\nu\rho} - q_\nu g_{\tau\rho})\left(\beta Q_{ab} - \frac{Q_\mathrm{c}}{m_\mathrm{c}}\,\delta_{ab}\right), \tag{176}$$

$$\Gamma^{(m)ab}_{\nu\rho}(q) = e\sqrt{mm_*}\varepsilon_{\nu\rho\alpha\beta}v^\alpha q^\beta\left(\beta Q_{ab} + \frac{Q_\mathrm{c}}{m_\mathrm{c}}\,\delta_{ab}\right), \tag{177}$$

where v_ν is the four-velocity of the heavy quark, $Q = \mathrm{diag}\,(2/3, -1/3)$ is the light-quark charge matrix, and m_c and $Q_\mathrm{c} = 2/3$ are the charmed quark mass and charge. The terms proportional to $Q_\mathrm{c}/m_\mathrm{c}$ come from the magnetic moment of the c quark and terms proportional to β are from the light-quark cloud in the D meson.

Thus, the radiative decay amplitude $\mathrm{X} \to \gamma\psi$ in the D-meson loop mechanism takes the form

$$M^{\mathrm{loop}} = \varepsilon^\nu(\psi)\varepsilon^\sigma(X)\varepsilon^\rho(\gamma)M^{\mathrm{loop}}_{\nu\sigma\rho}\,, \tag{178}$$

where

$$M^{\mathrm{loop}}_{\nu\sigma\rho} = \frac{1}{\sqrt{2}}\,ex_{\mathrm{nr}}g_2m\sqrt{M_\mathrm{X}m_\psi}I_{\nu\sigma\rho}\,, \tag{179}$$

with $I_{\nu\sigma\rho}$ given by the sum of the contributions from the individual diagrams in Fig. 18a–e. Amplitude (179) is gauge invariant, which is ensured by the transversality of magnetic vertices (176) and (177) as well as by the Ward identities.

The loop integral $I_{\nu\sigma\rho}$ in amplitude (179) is divergent. Therefore, we need to supply the amplitude with a counter term corresponding to the contact $\mathrm{X}\gamma\psi$ interaction (see the graph in Fig. 18f), which takes the form

$$M^{\mathrm{cont}} = \lambda\varepsilon_{\mu\sigma\rho\nu}\varepsilon^\mu(\psi)\varepsilon^\sigma(X)\varepsilon^\rho(\gamma)q^\nu\,, \tag{180}$$

and which is manifestly gauge invariant. To renormalize the model, we absorb the divergence of the loop into the bare constant λ providing the contact amplitude (180) with a finite strength λ_r.

Calculations were performed in the $\overline{\mathrm{MS}}$ [9] scheme for three values of the regularization scale: $\mu = M_\mathrm{X}/2$, $\mu = M_\mathrm{X}$, and $\mu = 2M_\mathrm{X}$. Given the uncertainties in the value of the coupling constant x_{nr} as well as in the constants g_2 and g_2' that define the coupling of the vector mesons J/ψ and ψ' to the D mesons, it is reasonable to introduce the ratios

$$r_x \equiv \left|\frac{x_{\mathrm{nr}}}{x^{(0)}_{\mathrm{nr}}}\right|, \qquad r_g \equiv \left|\frac{g_2}{g_2^{(0)}}\right|, \qquad r'_g \equiv \left|\frac{g_2'}{g_2^{(0)}}\right|, \tag{181}$$

where, as the starting point of model estimates, the values $|x^{(0)}_{\mathrm{nr}}| = 0.97\ \mathrm{GeV}^{-1/2}$ [138] and $|g_2^{(0)}| = 2\ \mathrm{GeV}^{-3/2}$ [139, 141] can be conveniently adopted.

The numerical results for the radiative decay widths and their ratio in the case $\lambda_\mathrm{r} = \lambda'_\mathrm{r} = 0$ are given in Table 7. We note that for $g_2'/g_2 \simeq 1$, the calculated ratio R is less than unity; however, it is much larger than the value obtained in Ref. [136]. On the other hand, the ratio $g_2'/g_2 \simeq 3$ is already sufficient to reproduce experimental ratio (16) even in the purely molecular picture.

Another source of uncertainty in the ratio R is the value of the renormalized contact interaction $\lambda_\mathrm{r}(\lambda'_\mathrm{r}) = 0$. Indeed, the requirement that the final result be renormalization-group invariant means that the variation in the loop contribution depending on the parameter μ is to be compensated by the corresponding variation in the contact term. The former, as seen from Table 7, is quite large, and hence, to compensate for it, the contribution of the contact term must be at least of the same order of magnitude, that is, must also be large. Thus, the radiative decays appear to be sensitive to the short-range part of the X(3872) wave function.

To estimate the contribution of the contact term, model considerations can be used. Because the most natural short-range contribution to the X(3872) wave function is provided by the genuine quark–antiquark state, we can find the ratio R by taking the estimates for the radiative decay widths of the $2^3\mathrm{P}_1$ $\bar{\mathrm{c}}\mathrm{c}$ charmonium in various quark models. Typical examples of such estimates are collected in Table 3, whence it can be seen that in spite of a large spread in the predictions, the values $\Gamma(\mathrm{X}(\bar{\mathrm{c}}\mathrm{c}) \to \gamma\mathrm{J}/\psi) \simeq 50$ keV and $\Gamma(\mathrm{X}(\bar{\mathrm{c}}\mathrm{c}) \to \gamma\psi') \simeq 100$ keV can be taken as natural ones, giving the ratio $R \simeq 2$.

We now recall that the relative weight of the quark and mesonic component and hence the contributions of the quark and meson loops are defined by the respective probabilities Z and $1 - Z$ (see the detailed discussion in Section 3). Thus, if we employ a more realistic model for X(3872) in which its wave function contains a sizable admixture of the charmonium with $Z \simeq 0.4-0.5$ (see the results in Section 5), then the experimental ratio R can be reproduced already for $g_2'/g_2 \simeq 2$, which is in line with the ratio of these couplings found in Ref. [135] and referring to the analysis in Ref. [139].

Thus, while the results of the calculations presented in Table 7 should be regarded only as order-of-magnitude estimates, two important conclusions can be drawn:

[9] The MS (minimal subtraction) renormalization scheme corresponds to dimensional regularization of loop integrals with a consequent omission of their divergent parts. In the modified $\overline{\mathrm{MS}}$ scheme, one additionally omits finite constants, which always accompany the divergent part of the integral.

Table 7. Calculated radiative decay widths $\Gamma(\mathrm{X} \to \gamma\psi)$ for $\psi = \mathrm{J}/\psi, \psi'$ and their ratio R.

	$\mu = M_{\mathrm{X}}/2$	$\mu = M_{\mathrm{X}}$	$\mu = 2M_{\mathrm{X}}$
$\Gamma(\mathrm{X} \to \gamma\mathrm{J}/\psi)$, keV	$9.7(r_x r_g)^2$	$23.5(r_x r_g)^2$	$43.2(r_x r_g)^2$
$\Gamma(\mathrm{X} \to \gamma\psi')$, keV	$3.8(r_x r'_g)^2$	$4.9(r_x r'_g)^2$	$6.0(r_x r'_g)^2$
$R = \dfrac{\Gamma(\mathrm{X} \to \gamma\psi')}{\Gamma(\mathrm{X} \to \gamma\mathrm{J}/\psi)}$	$0.39(g'_2/g_2)^2$	$0.21(g'_2/g_2)^2$	$0.14(g'_2/g_2)^2$

• The X(3872) radiative decays, in particular, the ratio of the widths R, are more sensitive to the short-range part of the X wave function than to the long-range part. Hence, these decays cannot be used to confirm or rule out the molecular model for the nature of X.

• The value of the ratio R of the order of unity and, in particular, its experimentally measured value (16) does not contradict the molecular picture for X(3872), in contrast to the prejudice existing in the literature based on early model estimates.

9. Conclusions

More than 60 years ago, Weinberg answered the question of whether the deuteron was a composite or elementary particle. While a relevant approach was developed and a proof was presented for the deuteron to be a proton–neutron molecule, reservations were outlined on the applicability of the approach to other hadronic resonances. To quote Weinberg, ''Nature is doing her best to keep us from learning whether the elementary particle deserves that title'' [40]. In most cases, Nature is indeed not very accommodating, but the X(3872) case offers a nice exception.

First and foremost, the X(3872) mass coincides almost exactly with the $\mathrm{D}^0\bar{\mathrm{D}}^{*0}$ threshold, which means that a sizable admixture of $\mathrm{D}\bar{\mathrm{D}}^*$ pairs in the X(3872) wave function is unavoidable, unless the coupling of X(3872) to those pairs is pathologically small. This threshold proximity allows us to develop a low-energy effective field theory, which in turn provides a systematic approach to the calculations of the production and decay processes for X(3872), thus investigating both long-range (molecular) and short-range (compact) components of the wave function.

Another important advantage of X(3872) is the existence of quark model predictions for the nearby $2^3\mathrm{P}_1$ bona fide charmonium, which constitutes the most natural candidate for the short-range part of the X(3872) wave function. Finally, the experimental situation is very friendly: detailed measurements of X(3872) production and decays are available, allowing us to test various model predictions. All this turns X(3872) from the enfant terrible of charmonium spectroscopy into a perfect laboratory for mesonic molecule studies.

The work by Yu S K was supported by the Ministry of Science and Education of the Russian Federation (grant 14.W03.31.0026); the work by A V N was supported by the Russian Science Foundation (grant 18-12-00226).

References

1. Eichten E et al. *Phys. Rev. D* **17** 3090 (1978); *Phys. Rev. D* **21** 313 (1980) Erratum
2. Pakhlova G V, Pakhlov P N, Eidel'man S I *Phys. Usp.* **53** 219 (2010); *Usp. Fiz. Nauk* **180** 225 (2010)
3. Choi S-K et al. (Belle Collab.) *Phys. Rev. Lett.* **91** 262001 (2003)
4. Tanabashi M et al. (Particle Data Group) *Phys. Rev. D* **98** 030001 (2018)
5. Kato Y et al. (Belle Collab.) *Phys. Rev. D* **97** 012005 (2018)
6. Abe K et al., in *Lepton and Photon Interactions at High Energies. Proc., 22nd Intern. Symp., LP 2005, Uppsala, Sweden, June 30 – July 5, 2005*
7. Choi S-K et al. *Phys. Rev. D* **84** 052004 (2011)
8. del Amo Sanchez P et al. (The BABAR Collab.) *Phys. Rev. D* **82** 011101(R) (2010)
9. Gokhroo G et al. (Belle Collab.) *Phys. Rev. Lett.* **97** 162002 (2006)
10. Aushev T et al. (Belle Collab.) *Phys. Rev. D* **81** 031103(R) (2010)
11. Aubert B et al. (BABAR Collab.) *Phys. Rev. D* **77** 011102(R) (2008)
12. Aubert B et al. (BABAR Collab.) *Phys. Rev. Lett.* **102** 132001 (2009)
13. Bhardwaj V et al. (Belle Collab.) *Phys. Rev. Lett.* **107** 091803 (2011)
14. Aaij R et al. (LHCb Collab.) *Nucl. Phys. B* **886** 665 (2014)
15. Abulencia A et al. (CDF Collab.) *Phys. Rev. Lett.* **98** 132002 (2007)
16. Hanhart C, Kalashnikova Yu S, Kudryavtsev A E, Nefediev A V *Phys. Rev. D* **85** 011501(R) (2012)
17. Aaij R et al. (LHCb Collab.) *Phys. Rev. Lett.* **110** 222001 (2013)
18. Aaij R et al. (LHCb Collab.) *Phys. Rev. D* **92** 011102(R) (2015)
19. Badalian A M, Morgunov V L, Bakker B L G *Phys. Atom. Nucl.* **63** 1635 (2000); *Yad. Fiz.* **63** 1722 (2000)
20. Barnes T, Godfrey S *Phys. Rev. D* **69** 054008 (2004)
21. Barnes T, Godfrey S, Swanson E S *Phys. Rev. D* **72** 054026 (2005)
22. Voloshin M B, Okun L B *JETP Lett.* **23** 333 (1976); *Pis'ma Zh. Eksp. Teor. Fiz.* **23** 369 (1976)
23. De Rújula A, Georgi H, Glashow S L *Phys. Rev. Lett.* **38** 317 (1977)
24. Törnqvist N A *Phys. Lett. B* **590** 209 (2004)
25. Törnqvist N A *Phys. Rev. Lett.* **67** 556 (1991)
26. Swanson E S *Phys. Lett. B* **588** 189 (2004)
27. Wong C-Y *Phys. Rev. C* **69** 055202 (2004)
28. Wang Z-G, Huang T *Eur. Phys. J. C* **74** 2891 (2014)
29. Kang X-W, Oller J A *Eur. Phys. J. C* **77** 399 (2017)
30. Suzuki M *Phys. Rev. D* **72** 114013 (2005)
31. Gamermann D, Oset E *Eur. Phys. J. A* **33** 119 (2007)
32. Maiani L et al. *Phys. Rev. D* **71** 014028 (2005)
33. Ebert D, Faustov R N, Galkin V O *Phys. Lett. B* **634** 214 (2006)
34. Ebert D et al. *Phys. Rev. D* **76** 114015 (2007)
35. Esposito A et al. *Int. J. Mod. Phys. A* **30** 1530002 (2015)
36. Dubynskiy S, Voloshin M B *Phys. Lett. B* **666** 344 (2008)
37. Dubynskiy S, Gorsky A, Voloshin M B *Phys. Lett. B* **671** 82 (2009)
38. Weinberg S *Phys. Rev.* **130** 776 (1963)
39. Weinberg S *Phys. Rev.* **131** 440 (1963)
40. Weinberg S *Phys. Rev.* **137** B672 (1965)
41. Guo F-K et al. *Rev. Mod. Phys.* **90** 015004 (2018)
42. Ablikim M et al. (BESIII Collab.) *Phys. Rev. Lett.* **110** 252001 (2013)
43. Liu Z Q et al. (Belle Collab.) *Phys. Rev. Lett.* **110** 252002 (2013)
44. Bondar A et al. (Belle Collab.) *Phys. Rev. Lett.* **108** 122001 (2012)
45. Garmash A et al. (Belle Collab.) *Phys. Rev. Lett.* **116** 212001 (2016)
46. Bondar A E et al. *Phys. Rev. D* **84** 054010 (2011)
47. Aubert B et al. (BABAR Collab.) *Phys. Rev. Lett.* **95** 142001 (2005)
48. Wang Q, Hanhart C, Zhao Q *Phys. Rev. Lett.* **111** 132003 (2013)
49. Wang Q et al. *Phys. Rev. D* **89** 034001 (2014)
50. Cleven M et al. *Phys. Rev. D* **90** 074039 (2014)
51. Wu X-G et al. *Phys. Rev. D* **89** 054038 (2014)
52. Guo F-K et al. *Phys. Lett. B* **725** 127 (2013)
53. Baru V et al. *Phys. Lett. B* **586** 53 (2004)
54. Baz'A I, Zel'dovich Ya B, Perelomov A M *Scattering, Reactions and Decay in Nonrelativistic Quantum Mechanics* (Jerusalem: Israel Program for Scientific Translations, 1969); Translated from Russian: *Rasseyanie, Reaktsii i Raspady v Nerelyativistskoi Kvantovoi Mekhanike* (Moscow: Nauka, 1971)
55. Baru V et al. *Eur. Phys. J. A* **44** 93 (2010)
56. Hanhart C, Kalashnikova Yu S, Nefediev A V *Eur. Phys. J. A* **47** 101 (2011)
57. Landau L D, Lifshitz E M *Quantum Mechanics. Non-Relativistic Theory* (Oxford: Pergamon Press, 1977); Translated from Russian: *Kvantovaya Mekhanika. Nerelyativistskaya Teoriya* (Moscow: Fizmatlit, 2004)
58. Bogdanova L N, Hale G M, Markushin V E *Phys. Rev. C* **44** 1289 (1991)

59. Flatté S M *Phys. Lett. B* **63** 224 (1976)
60. Landau L D *Sov. Phys. JETP* **12** 1294 (1961); *Zh. Eksp. Teor. Fiz.* **39** 1856 (1960)
61. Morgan D *Nucl. Phys. A* **543** 632 (1992)
62. Artoisenet P, Braaten E, Kang D *Phys. Rev. D* **82** 014013 (2010)
63. Braaten E, Stapleton J *Phys. Rev. D* **81** 014019 (2010)
64. Micu L *Nucl. Phys. B* **10** 521 (1969)
65. Le Yaouanc A et al. *Phys. Rev. D* **8** 2223 (1973)
66. Busetto G, Oliver L *Z. Phys. C* **20** 247 (1983)
67. Kokoski R, Isgur N *Phys. Rev. D* **35** 907 (1987)
68. Barnes T et al. *Phys. Rev. D* **55** 4157 (1997)
69. Ackleh E S, Barnes T, Swanson E S *Phys. Rev. D* **54** 6811 (1996)
70. Di Giacomo A et al. *Phys. Rep.* **372** 319 (2002)
71. Simonov Yu A *Phys. Atom. Nucl.* **66** 2033 (2003); *Yad. Fiz.* **66** 2083 (2003)
72. Kalashnikova Yu S *Phys. Rev. D* **72** 034010 (2005)
73. Danilkin I V, Simonov Yu A *Phys. Rev. D* **81** 074027 (2010)
74. Danilkin I V, Simonov Yu A *Phys. Rev. Lett.* **105** 102002 (2010)
75. Badalyan A M et al. *Phys. Rep.* **82** 31 (1982)
76. Barnes T, Swanson E S *Phys. Rev. C* **77** 055206 (2008)
77. AlFiky M T, Gabbiani F, Petrov A A *Phys. Lett. B* **640** 238 (2006)
78. Voloshin M B *Phys. Rev. D* **84** 031502(R) (2011)
79. Mehen T, Powell J W *Phys. Rev. D* **84** 114013 (2011)
80. Ohkoda S et al. *Phys. Rev. D* **86** 014004 (2012)
81. Pavón Valderrama M *Phys. Rev. D* **85** 114037 (2012)
82. Hidalgo-Duque C, Nieves J, Pavón Valderrama M *Phys. Rev. D* **87** 076006 (2013)
83. Nieves J, Pavón Valderrama M *Phys. Rev. D* **86** 056004 (2012)
84. Guo F-K et al. *Phys. Rev. D* **88** 054007 (2013)
85. Baru V et al. *J. High Energ. Phys.* **2017** 158 (2017)
86. Hidalgo-Duque C et al. *Phys. Lett. B* **727** 432 (2013)
87. Albaladejo M et al. *Eur. Phys. J. C* **75** 547 (2015)
88. Baru V et al. *Phys. Lett. B* **763** 20 (2016)
89. Braaten E, Kusunoki M *Phys. Rev. D* **71** 074005 (2005)
90. Bignamini C et al. *Phys. Rev. Lett.* **103** 162001 (2009)
91. Albaladejo M et al. *Chinese Phys. C* **41** 121001 (2017)
92. Esposito A et al. *Chin. Phys. C* **42** 114107 (2018)
93. Kalashnikova Yu S, Nefediev A V *Phys. Rev. D* **80** 074004 (2009)
94. Kalashnikova Yu S, Kudryavtsev A E, Nefediev A V *Phys. Atom. Nucl.* **73** 1592 (2010); *Yad. Fiz.* **73** 1638 (2010)
95. Meng C, Gao Y-J, Chao K-T *Phys. Rev. D* **87** 074035 (2013)
96. Aubert B et al. (BABAR Collab.) *Phys. Rev. D* **74** 011106(R) (2006)
97. Badalian A M et al. *Phys. Rev. D* **85** 114002 (2012)
98. Badalian A M, Simonov Yu A, Bakker B L G *Phys. Rev. D* **91** 056001 (2015)
99. Adachi I et al., in *Proc. of 34th Intern. Conf. on High Energy Physics, ICHEP 2008, Philadelphia, Pennsylvania, July 30 – August 5, 2008* (Stanford: SLAC, 2008)
100. Aubert B et al. (BABAR Collab.) *Phys. Rev. D* **77** 111101 (2008)
101. Hanhart C, Kalashnikova Yu S, Kudryavtsev A E, Nefediev A V *Phys. Rev. D* **76** 034007 (2007)
102. Bugg D V *J. Phys. G* **35** 075005 (2008)
103. Hanhart C, Kalashnikova Yu S, Nefediev A V *Phys. Rev. D* **81** 094028 (2010)
104. Nauenberg M, Pais A, PRINT-64-554 (1964)
105. Braaten E, Lu M *Phys. Rev. D* **76** 094028 (2007)
106. Voloshin M B *Phys. Lett. B* **579** 316 (2004)
107. Baru V et al. *Phys. Rev. D* **84** 074029 (2011)
108. Filin A A et al. *Phys. Rev. Lett.* **105** 019101 (2010)
109. Close F, Downum C *Phys. Rev. Lett.* **102** 242003 (2009)
110. Close F, Downum C, Thomas C E *Phys. Rev. D* **81** 074033 (2010)
111. Liu Y-R et al. *Eur. Phys. J. C* **56** 63 (2008)
112. Thomas C E, Close F E *Phys. Rev. D* **78** 034007 (2008)
113. Kalashnikova Yu S, Nefediev A V *JETP Lett.* **97** 70 (2013); *Pis'ma Zh. Eksp. Teor. Fiz.* **97** 76 (2013)
114. Novozhilov Yu V *Introduction to Elementary Particle Theory* (Oxford: Pergamon Press, 1975); Translated from Russian: *Vvedenie v Teoriyu Elementarnykh Chastits* (Moscow: Nauka, 1972)
115. Kalashnikova Yu S, Nefediev A V *Phys. Atom. Nucl.* **60** 1389 (1997); *Yad. Fiz.* **60** 1529 (1997)
116. Baru V et al. *Phys. Rev. D* **91** 034002 (2015)
117. Nogga A, Timmermans R G E, van Kolck U *Phys. Rev. C* **72** 054006 (2005)
118. Kudryavtsev A E, Markushin V E, Shapiro I S *Sov. Phys. JETP* **47** 225 (1978); *Zh. Eksp. Teor. Fiz.* **47** 432 (1978)
119. Kudryavtsev A E, Popov V S *JETP Lett.* **29** 280 (1979); *Pis'ma Zh. Eksp. Teor. Fiz.* **29** 311 (1979)
120. Beane S R et al. *Nucl. Phys. A* **700** 377 (2002)
121. Braaten E, Phillips D *Phys. Rev. A* **70** 052111 (2004)
122. Fleming S et al. *Phys. Rev. D* **76** 034006 (2007)
123. Kaplan D B, Savage M J, Wise M B *Nucl. Phys. B* **534** 329 (1998)
124. Nieves J, Pavón Valderrama M P *Phys. Rev. D* **84** 056015 (2011)
125. Guo F-K et al. *Eur. Phys. J. C* **74** 2885 (2014)
126. Prelovsek S, Leskovec L *Phys. Rev. Lett.* **111** 192001 (2013)
127. Lee S et al., arXiv:1411.1389
128. Padmanath M, Lang C B, Prelovsek S *Phys. Rev. D* **92** 034501 (2015)
129. Jansen M, Hammer H-W, Jia Y *Phys. Rev. D* **92** 114031 (2015)
130. Gell-Mann M, Oakes R J, Renner B *Phys. Rev.* **175** 2195 (1968)
131. Baru V et al. *Phys. Lett. B* **726** 537 (2013)
132. Baru V et al. *Phys. Rev. D* **92** 114016 (2015)
133. Dong Y et al. *Phys. Rev. D* **77** 094013 (2008)
134. Dong Y et al. *Phys. Rev. D* **79** 094013 (2009)
135. Dong Y et al. *J. Phys. G* **38** 015001 (2011)
136. Swanson E S *Phys. Lett. B* **598** 197 (2004)
137. Guo F-K et al. *Phys. Lett. B* **742** 394 (2015)
138. Guo F-K et al. *Phys. Lett. B* **725** 127 (2013)
139. Colangelo P, De Fazio F, Pham T N *Phys. Rev. D* **69** 054023 (2004)
140. Guo F-K, Hanhart C, Meißner U-G *Phys. Rev. Lett.* **103** 082003 (2009); *Phys. Rev. Lett.* **104** 109901 (2010) Erratum
141. Guo F-K et al. *Phys. Rev. D* **83** 034013 (2011)
142. Amundson J F et al. *Phys. Lett. B* **296** 415 (1992)
143. Cheng H-Y et al. *Phys. Rev. D* **47** 1030 (1993)